



Atmospheric Correction of Land Remote Sensing Data and Algorithm Updates

Eric Vermote

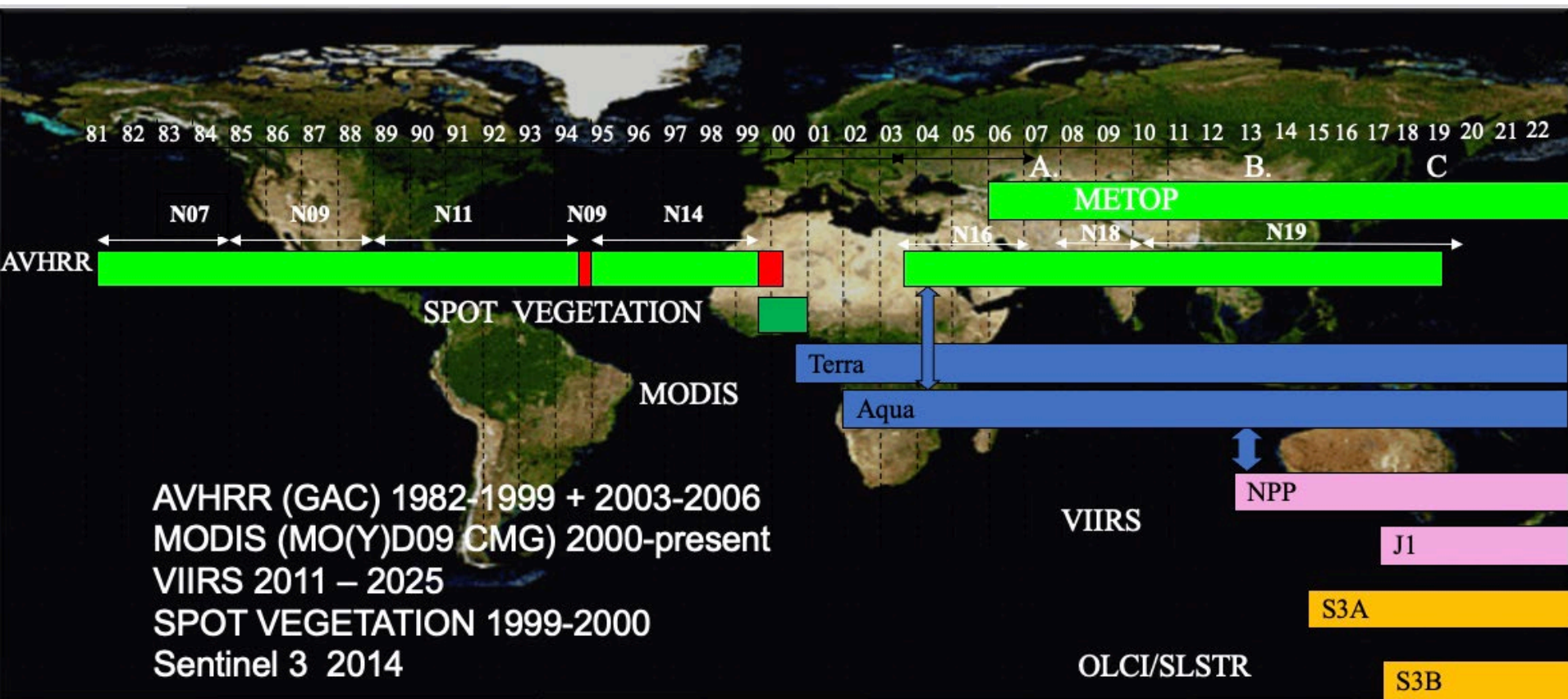
NASA Goddard Space Flight Center Code 619

Eric.f.vermote@nasa.gov



A Land Climate Data Record

Multi instrument/Multi sensor Science Quality Data Records used to quantify trends and changes



<https://ltdr.modaps.eosdis.nasa.gov>
Emphasis on data consistency – characterization rather than degrading/smoothing the data

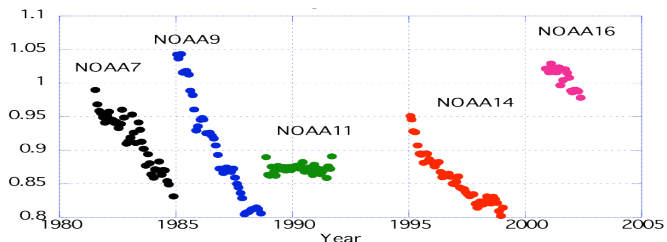


Land Climate Data Record (Approach)

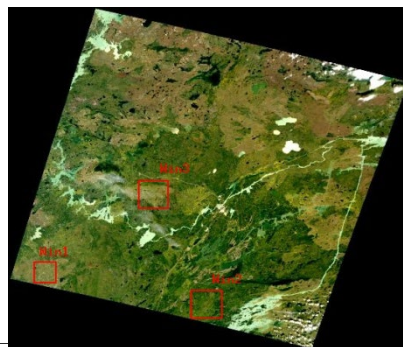
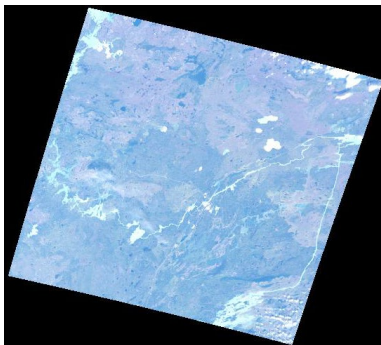
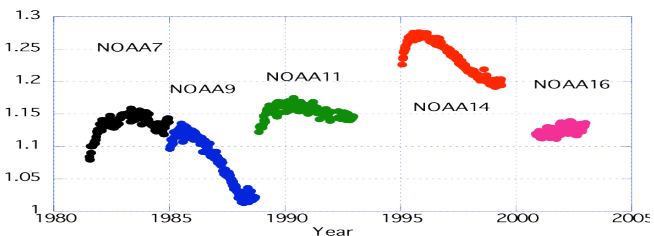
Needs to address geolocation, calibration, atmospheric/BRDF correction issues

CALIBRATION

Degradation in channel 1
(from Ocean observations)

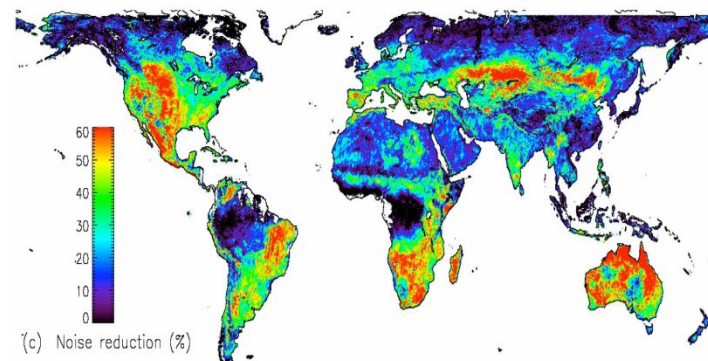
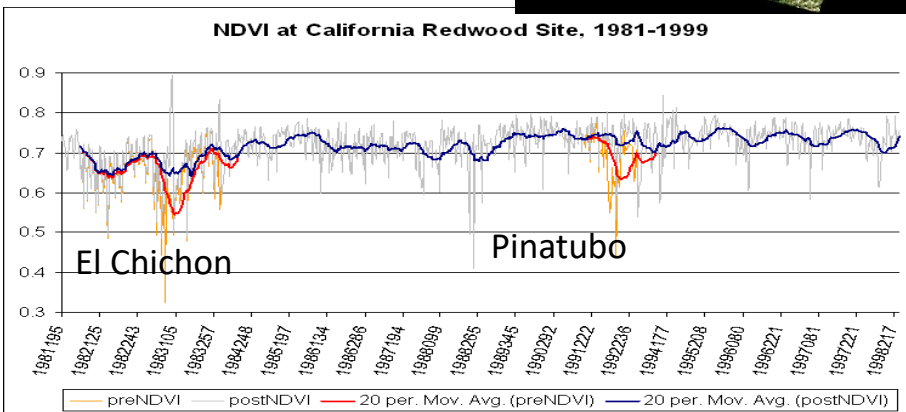
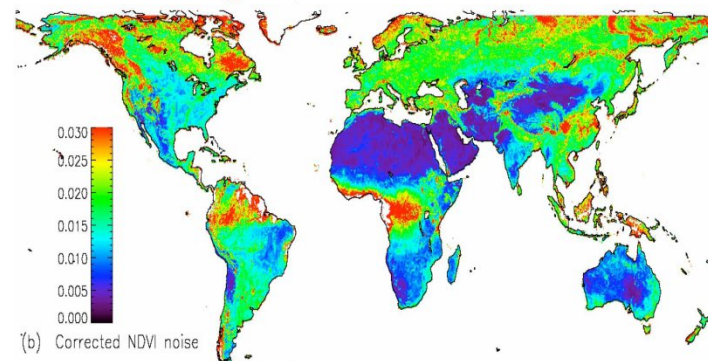
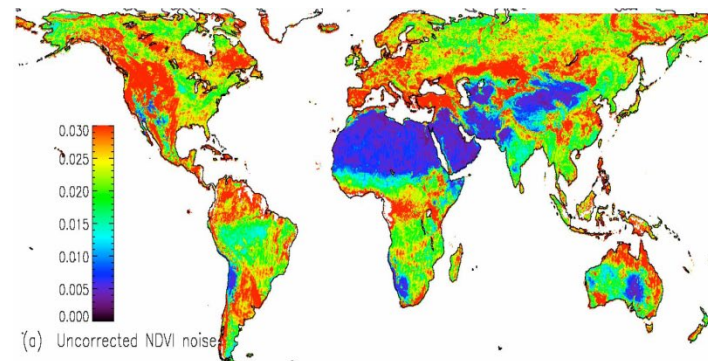


Channel1/Channel2 ratio
(from Clouds observations)



ATMOSPHERIC CORRECTION

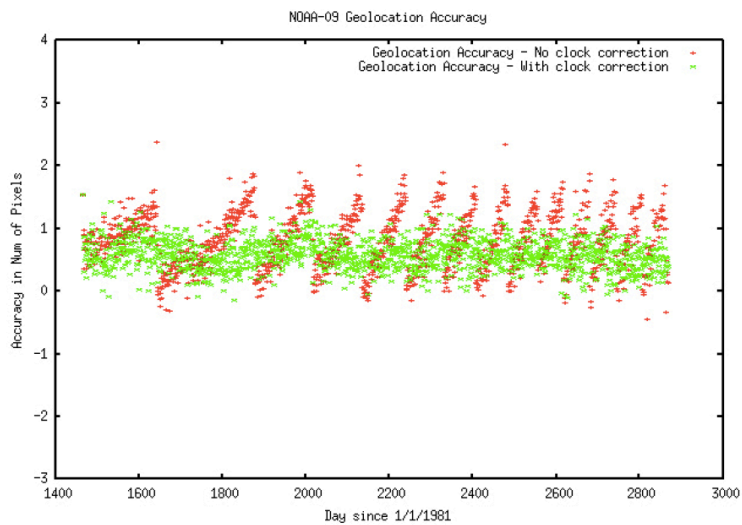
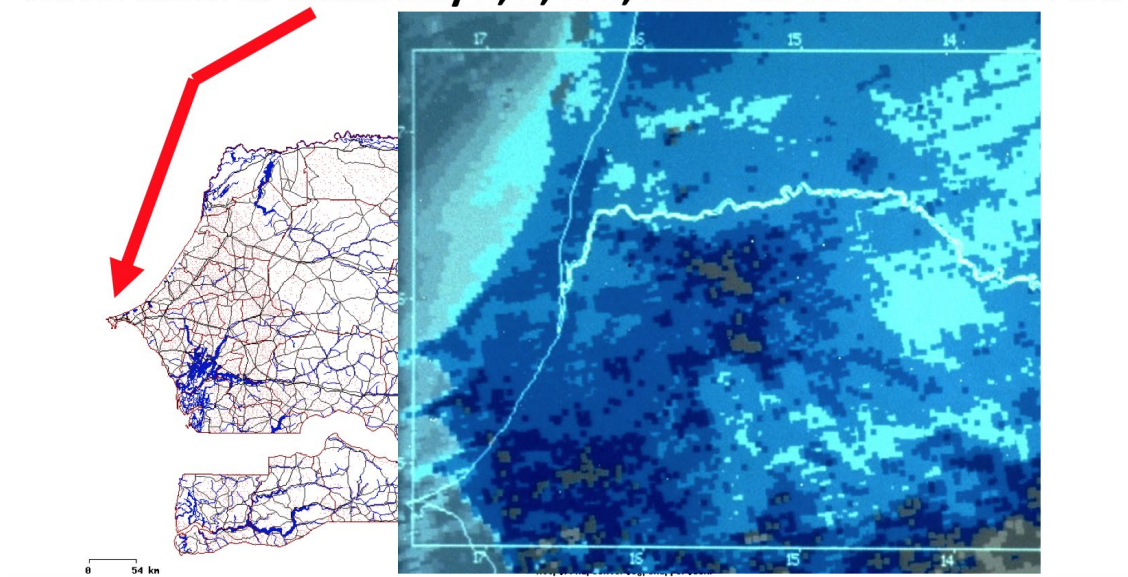
BRDF CORRECTION





AVHRR GEOLOCATION

Three Cities of Dakar July 1, 2, & 3, 1981 NOAA-7 AVHRR 1 km



From Franch et al., 2017

Figure 2. Accuracy assessment of the geolocation of AVHRR products using the coastal chips database (in fraction of pixels). Green is with clock correction, and red is without clock correction.



AVHRR CALIBRATION

INT. J. REMOTE SENSING, 1995, VOL. 16, NO. 13, 2317-2340

Absolute calibration of AVHRR visible and near-infrared channels using ocean and cloud views

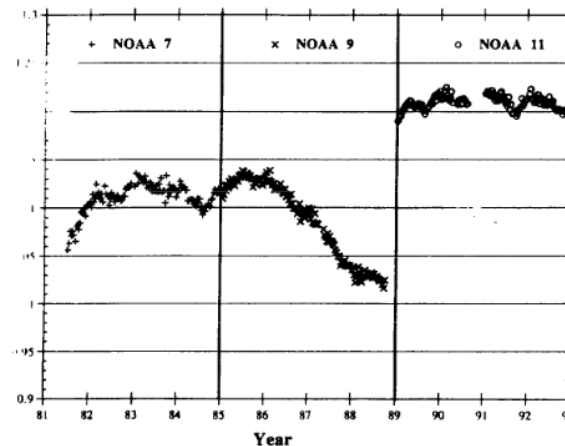
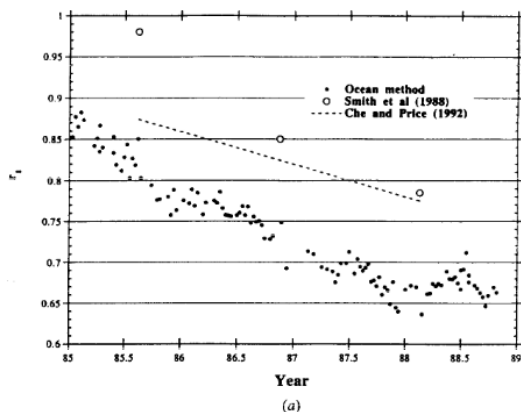
E. VERMOTE

Laboratory for Global Remote Sensing, Lefrak Hall, University of Maryland, College Park Maryland, U.S.A.

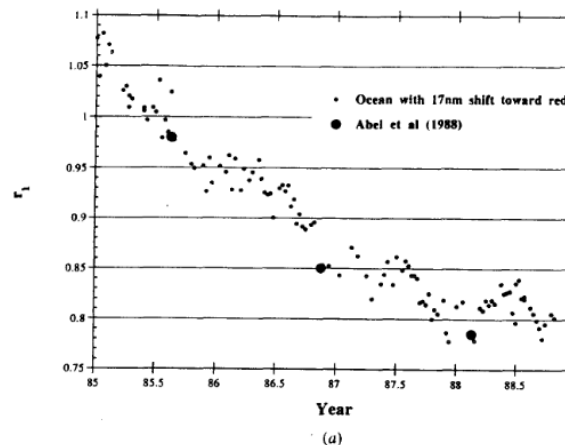
and Y. J. KAUFMAN

Laboratory for Atmospheres Code 913, NASA/GSFC, Greenbelt MD 20771, U.S.A.

(Received 8 February 1994; in final form 21 August 1994)



Ratio between the deterioration of channels 1 and 2, r_{12} as observed over high reflective clouds for NOAA-7, -9, -11.





AVHRR CALIBRATION

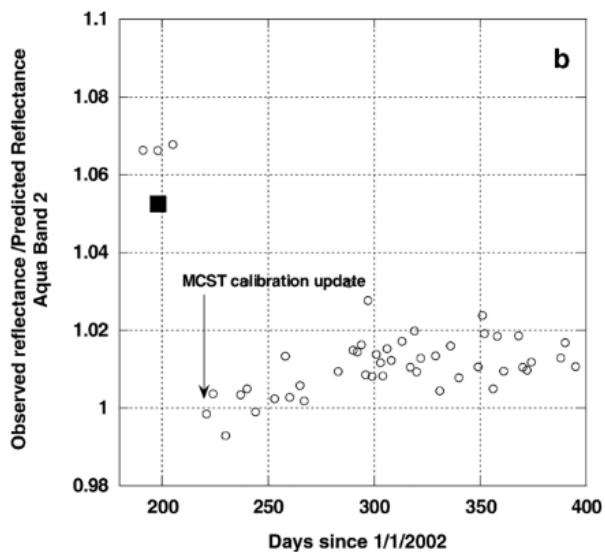
Calibration of NOAA16 AVHRR over a desert site using MODIS data

E.F. Vermote ^{a,*}, N.Z. Saleous ^b

^a University of Maryland, Department of geography and NASA GSFC Code 614.5, United States

^b SAIC and NASA GSFC Code 614.5, United States

Received 24 February 2006; received in revised form 16 June 2006; accepted 27 June 2006



■ MCST ratio preflight to solar diffuser calibration

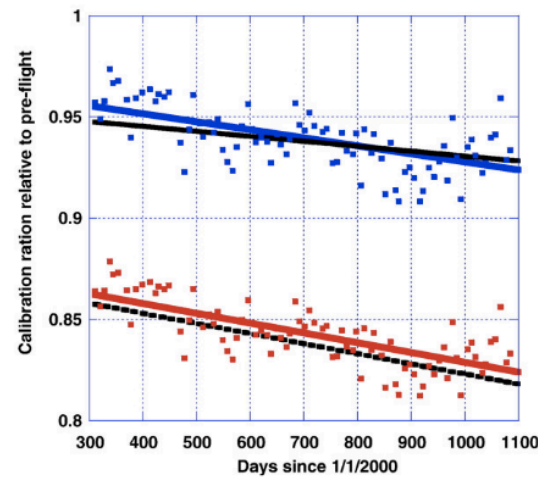


Fig. 11. Comparison of the desert calibration trends for band 1 (black solid line) and band 2 (black interrupted line), with the trends obtained using the Ocean and Clouds method (Vermote and Kaufman, 1995) for band 1 (blue line and square) and band 2 (red line and square).

D20105

CAO ET AL.: AVHRR LUNAR NDVI FOR CLIMATE CHANGE

D20105

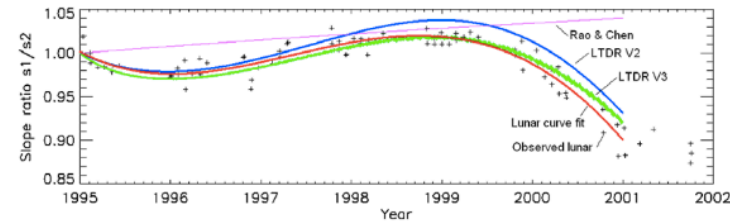


Figure 3. Comparison of the long-term trend of slope ratio for NOAA 14 between lunar, LTDR, and NOAA operational (red, lunar curve fit; pluses, lunar observation; green, LTDR version 3; blue, LTDR version 2; and pink, NOAA operational).



Article

A 30+ Year AVHRR Land Surface Reflectance Climate Data Record and Its Application to Wheat Yield Monitoring

Belen Franch ^{1,2,*}, Eric F. Vermote ², Jean-Claude Roger ^{1,2}, Emilie Murphy ^{1,2}, Inbal Becker-Reshef ¹, Chris Justice ¹, Martin Claverie ^{1,2}, Jyoteshwar Nagol ¹, Ivan Csizsar ³, Dave Meyer ⁴, Frederic Baret ⁵, Edward Masuoka ², Robert Wolfe ² and Sadashiva Devadiga ⁶

- ¹ Department of Geographical Sciences, University of Maryland, College Park, MD 20742, USA; roger63@umd.edu (J.-C.R.); emilie.murphy@nasa.gov (E.M.); ireshf@umd.edu (I.B.-R.); cjustice@umd.edu (C.J.); mcl@umd.edu (M.C.); jnagol@umd.edu (J.N.)
 - ² NASA Goddard Space Flight Center, 8800 Greenbelt Road, Greenbelt, MD 20771, USA; eric.f.vermote@nasa.gov (E.F.V.); edward.j.masuoka@nasa.gov (E.M.); robert.e.wolfe@nasa.gov (R.W.); Ivan.Csizsar@noaa.gov
 - ³ NOAA Center for Satellite Applications and Research, College Park, MD 20746, USA;
 - ⁴ Goddard Earth Science Data and Information Services Center (GES DISC), NASA Goddard Space Flight Center, 8800 Greenbelt Road, Greenbelt, MD 20771, USA; david.j.meyer@nasa.gov
 - ⁵ INRA, Unité Environnement Méditerranéen et Modélisation des Agro-Hydrosystèmes (UMR1114), Domaine St Paul, Site Agroparc, 84914 Avignon CEDEX 09, France; frederic.baret@avignon.inra.fr
 - ⁶ Science Systems and Applications Inc., Lanham, MD 20706, USA; sadashiva.devadiga-1@nasa.gov
- * Correspondence: belen.franchgras@nasa.gov

Academic Editors: Jose Moreno, Clement Atzberger and Prasad S. Thenkabail
Received: 27 May 2016; Accepted: 15 March 2017; Published: 21 March 2017

AVHRR CALIBRATION

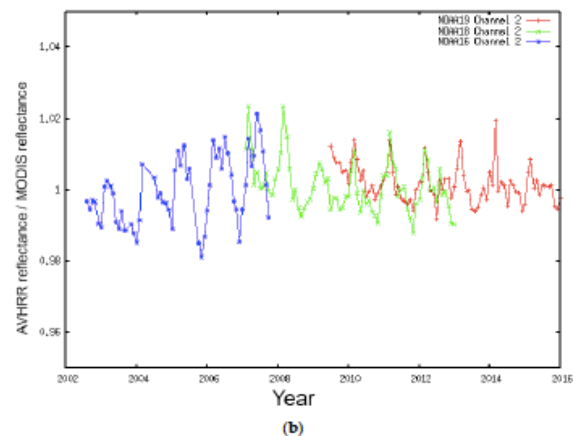
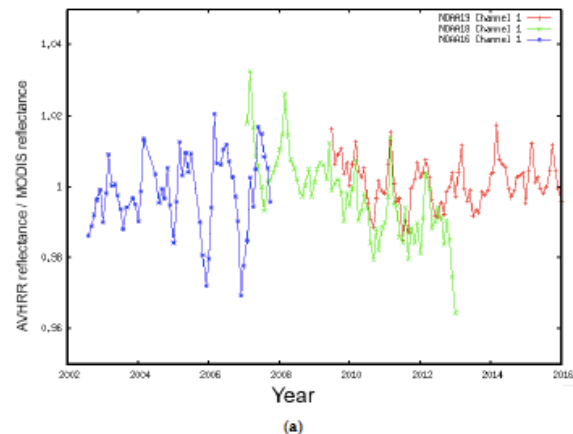
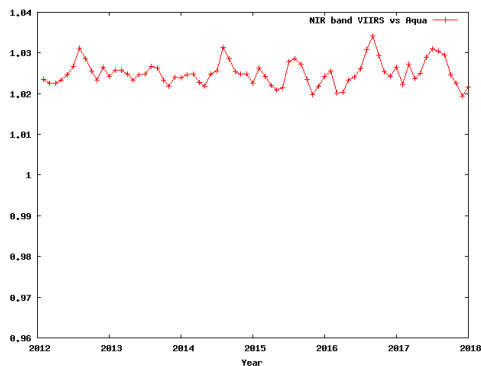
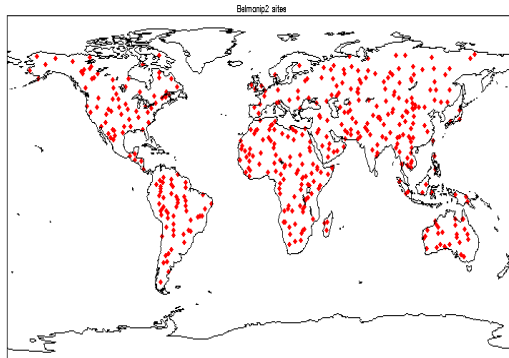


Figure 7. Cross-comparison between AVHRR N16, N18, and N19 and MODIS Terra ratios for the BELMANIP2 sites for the red band (a) and the near infrared band (b).



BELMANIP sites



Automated monthly VIIRS cross comparison (over BELMANIP sites) with MODIS Aqua from 2012. the stability of both VIIRS and MODIS Aqua is excellent in both red and NIR as shown (+/- 0.5%).



AVHRR ATMOSPHERIC CORRECTION EVOLUTION

Pathfinder I: Partial correction

James, M.E. and Kalluri, S.N., 1994. The Pathfinder AVHRR land data set: An improved coarse resolution data set for terrestrial monitoring. *International Journal of Remote Sensing*, 15(17), pp.3347-3363.

Pathfinder II: Improved correction fixed Pathfinder I issues

El Saleous, N.Z., Vermote, E.F., Justice, C.O., Townshend, J.R.G., Tucker, C.J. and Goward, S.N., 2000. Improvements in the global biospheric record from the Advanced Very High Resolution Radiometer (AVHRR). *International Journal of Remote Sensing*, 21(6-7), pp.1251-1277.

LTDR (Version 2.,3., 4.): Improvement on going, water vapor correction, aerosol correction.

Franch, B., Vermote, E., Roger, J.C., Murphy, E., Becker-Reshef, I., Justice, C., Claverie, M., Nagol, J., Csiszar, I., Meyer, D. and Baret, F., 2017. A 30+ year AVHRR land surface reflectance climate data record and its application to wheat yield monitoring. *Remote Sensing*, 9(3), p.296



DATA PRODUCTS

Production/Distribution

- *AVHRR NOAA/METOP V5 – MODIS C6.1 – VIIRS C2*
- Daily Surface reflectance's at nadir, sun at 45deg in Red, NIR and 3.75mic (experimental), NDVI, LAI/FAPAR, Cloud Mask, TOA Brightness temperature at 11mic and 12mic

Development

- *Sentinel 3 (OLCI/SLSTR)*
- Daily Albedo, Improved Cloud/Snow Mask, Spectral Adjustment, Improved BDRF/ Atmospheric correction (Water vapor), Global Validation/Accuracy Assesment.



AVHRR LTDR APPLICATIONS

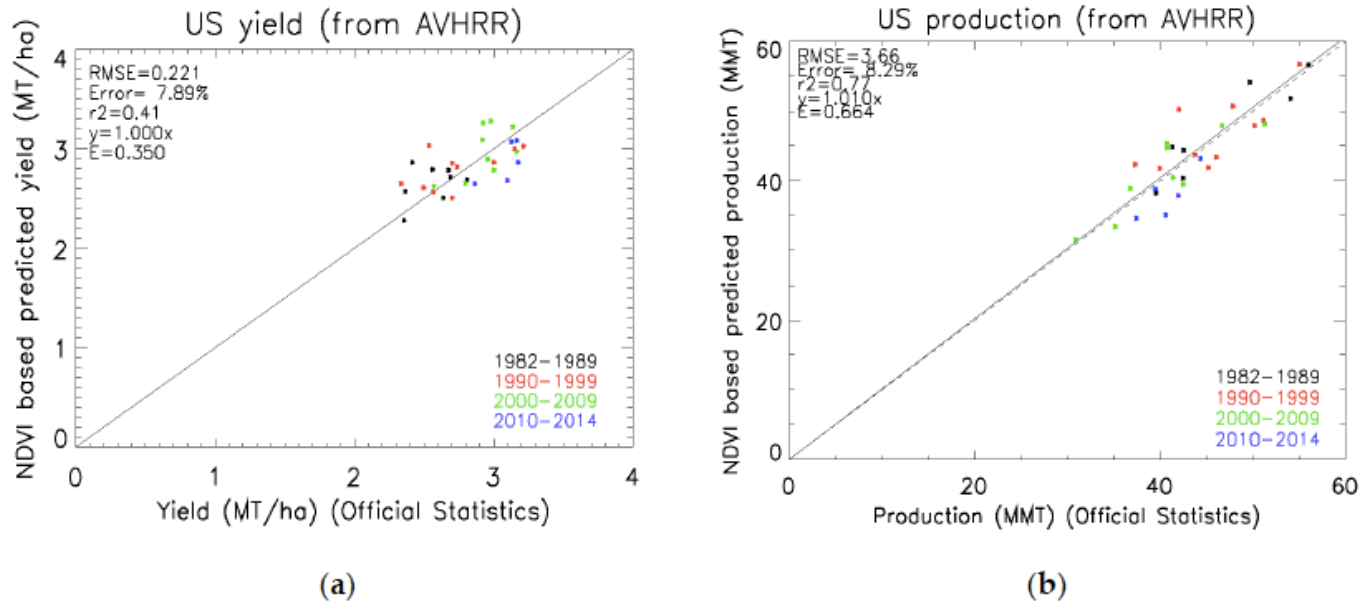


Figure 9. National winter wheat predicted yield (a) and production (b) in the U.S., applying the 'original' method [1] to AVHRR data plotted against USDA-reported statistics (<https://quickstats.nass.usda.gov>).




AVHRR LTDR APPLICATIONS



Letter | Published: 08 August 2018

Global land change from 1982 to 2016

Xiao-Peng Song , Matthew C. Hansen, Stephen V. Stehman, Peter V. Potapov, Alexandra Tyukavina, Eric F. Vermote & John R. Townshend

Here we analyse 35 years' worth of satellite data and provide a comprehensive record of global land-change dynamics during the period 1982–2016. We show that—contrary to the prevailing view that forest area has declined globally⁵—tree cover has increased by 2.24 million km² (+7.1% relative to the 1982 level). This overall net gain is the result of a net loss in the tropics being outweighed by a net gain in the extratropics.

Extended Data Table 1 Estimates of 1982 land-cover area and 1982–2016 land-cover change at continental and global scales

From: Global land change from 1982 to 2016

Continent	Tree canopy cover						Short vegetation cover						Bare ground cover								
	Annual net change			Gross change			Annual net change			Gross change			Annual net change			Gross change					
	Area 1982 (10 ³ km ²)	Slope (10 ³ km ² yr ⁻¹)	Lower (10 ³ km ² yr ⁻¹)	Upper (10 ³ km ² yr ⁻¹)	p	loss (10 ³ km ²)	gain (10 ³ km ²)	Area 1982 (10 ³ km ²)	Slope (10 ³ km ² yr ⁻¹)	Lower (10 ³ km ² yr ⁻¹)	Upper (10 ³ km ² yr ⁻¹)	p	loss (10 ³ km ²)	gain (10 ³ km ²)	Area 1982 (10 ³ km ²)	Slope (10 ³ km ² yr ⁻¹)	Lower (10 ³ km ² yr ⁻¹)	Upper (10 ³ km ² yr ⁻¹)	p	loss (10 ³ km ²)	gain (10 ³ km ²)
Africa	4672	-1.9	-7.6	3.6	0.609	-267	262	11653	14.8	6.5	23.2	0.016	-268	571	13413	-12.4	-19.9	-4.7	0.020	-371	105
Asia	8457	37.5	28.0	45.3	0.000	-178	1170	21774	-22.9	-34.5	-9.6	0.008	-1261	760	13926	-15.1	-23.1	-7.4	0.002	-798	358
Europe	2719	28.3	20.4	32.8	0.000	-17	758	6320	-22.0	-27.3	-14.7	0.000	-673	50	668	-4.3	-5.8	-2.6	0.000	-92	9
North America	5815	15.6	3.5	24.2	0.020	-205	583	12921	-12.7	-4.1	-2.2	0.031	-594	286	4847	-2.5	-7.3	2.2	0.363	-186	140
South America	8767	-14.1	-20.5	-7.4	0.001	-621	190	7165	14.8	8.1	21.0	0.002	-224	655	1717	1.9	-1.2	3.8	0.307	-92	102
Oceania	680	0.1	-1.4	1.7	0.887	-40	56	4800	-4.4	-12.1	3.4	0.349	-132	50	2772	5.2	-3.9	12.5	0.280	-35	113
Global	31628	66.0	27.3	100.5	0.008	-1331	3039	64539	-26.0	-64.8	15.2	0.244	-3170	2380	37412	-34.0	-52.3	-10.0	0.023	-1582	830

Annual net change in land cover (slope) and 1982 land-cover area were estimated using Theil–Sen regression of the time series of annual land-cover area per continent or over the globe (excluding Antarctica). Lower and upper slopes represent the 90% confidence interval. Reported P value is for the two-sided Mann–Kendall test for trend, with $P < 0.05$ used to define statistical significance, and a sample size of $n = 35$ years. Gross change in land cover was estimated on the basis of per-pixel non-parametric trend analysis. Per-pixel loss and gain were summed to derive gross loss and gain at the aggregated scales.



Generic Surface reflectance algorithm

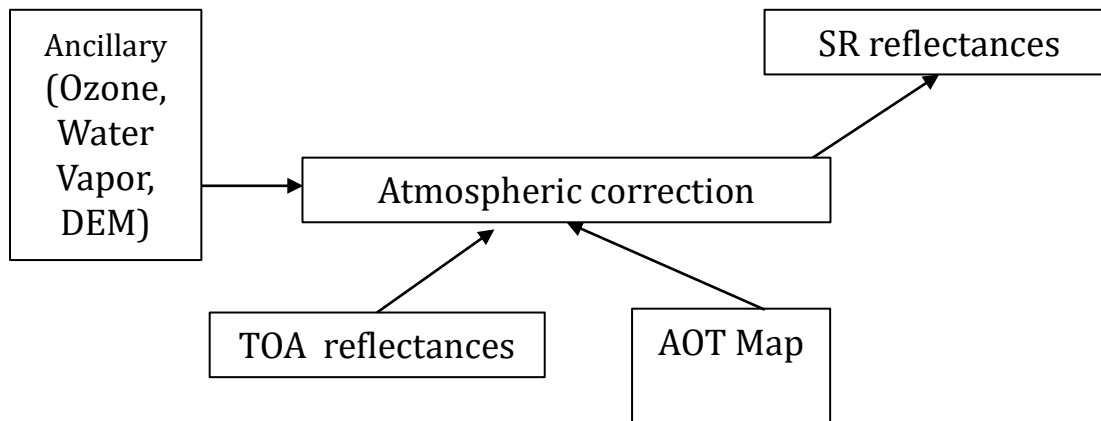
The Surface reflectance algorithm relies on

- the use of very accurate (better than 1%) vector radiative transfer modeling of the coupled atmosphere-surface system
- the inversion of key atmospheric parameters (aerosol, water vapor)

Home page: <http://modis-sr.ltdri.org>



Generic flowchart for atmospheric correction





Generic Aerosol inversion

Reading Inputs, LUT and Ancillary data

ρ_{surf} determined (*) using ρ_{atm} , T_{atm} and S_{atm} from LUT assuming AOT, Aerosol model and knowing pressure, altitude, water vapor, ozone...

Using an assumed relationship between the blue surface reflectance (~450nm) and the red surface reflectance (~650nm) and fixing the aerosol model we are able to retrieve the AOT.

We loop the AOT until $(\rho_{surf} \text{ blue} / \rho_{surf} \text{ red})_{derived} = (\rho_{surf} \text{ blue} / \rho_{surf} \text{ red})_{assumed}$

The retrieved AOT is used to compute the surface reflectance at other wavelengths in the blue and SWIR to make a more robust inversion and refine the aerosol model. by minimizing the residual.

$$residual = \frac{\sum_{i=1}^2 (\rho_{surf}^i - Ratio_{665}^i * \rho_{surf}^{665})}{2}$$

Aerosol Opt. Thick. and Aerosol model for each pixel

Surface reflectance for each pixel and each band

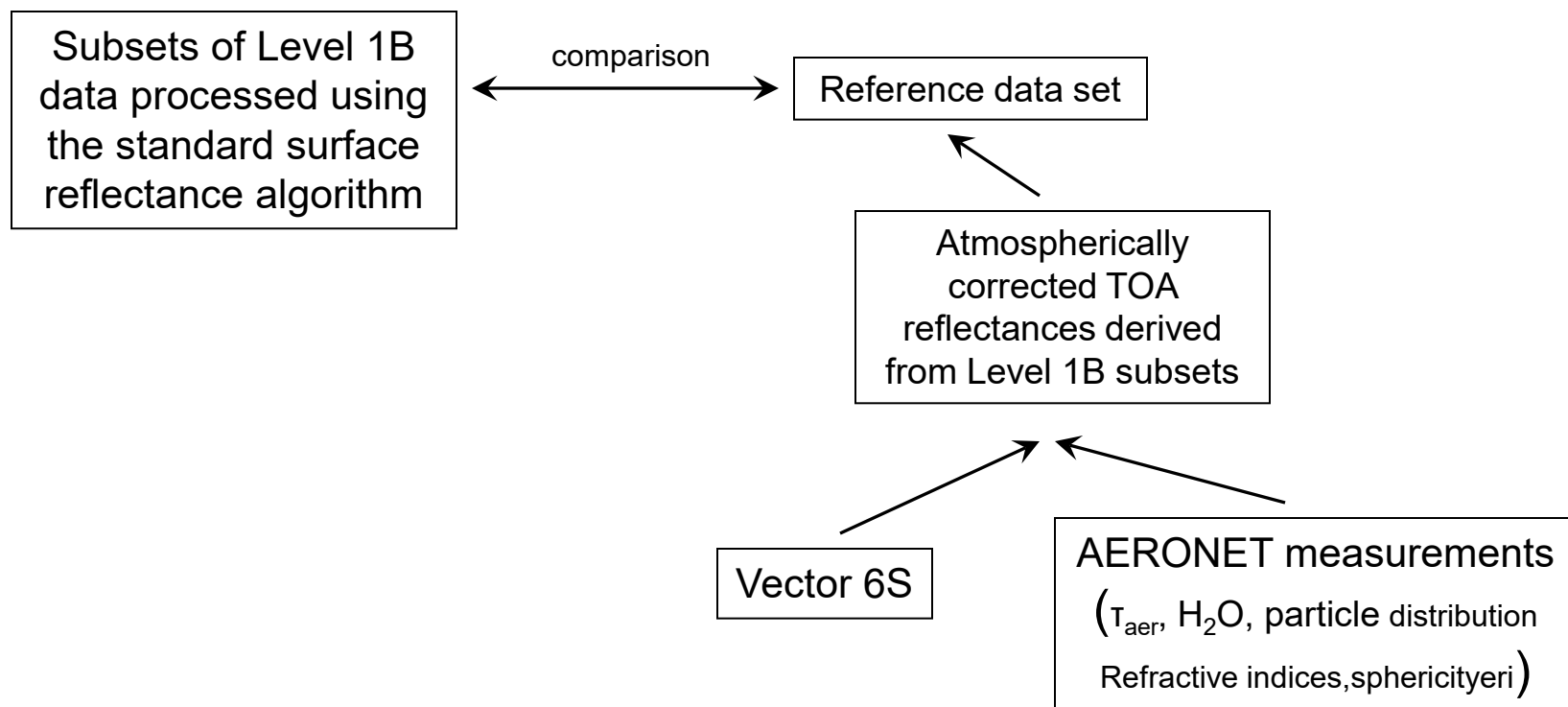
Computation of surface reflectances for all channels

ρ_{surf} determined (*) using ρ_{atm} , T_{atm} and S_{atm} from LUT knowing AOT, Aerosol model, pressure, altitude, water vapor, ozone...

$$(*) \rho_{surf} = \frac{Y}{1 + S_{atm} \cdot Y} \quad \text{with} \quad Y = \frac{1}{T_{atm} \cdot tg^{wv}} \left[\left(\frac{\rho_{TOA}}{tg^{O3} \cdot tg^{others}} \right) - (\rho_{atm} - \rho_{ray}) \cdot tg^{wv/2} - \rho_{ray} \right]$$

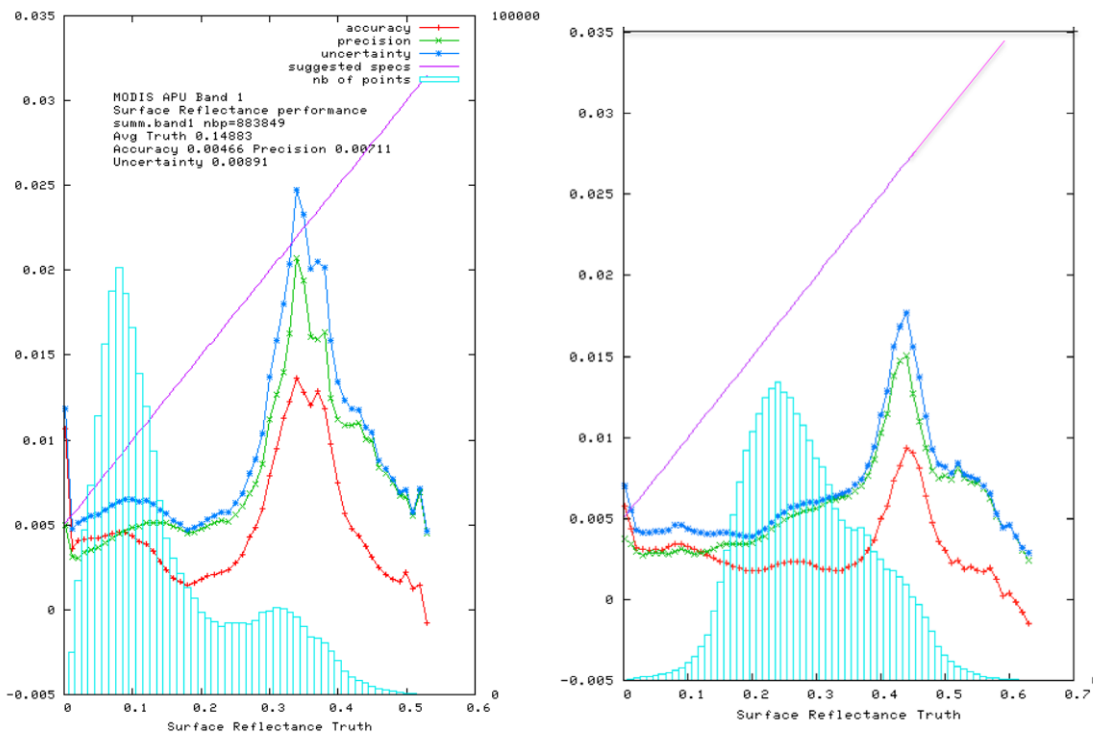


Methodology for evaluating the performance of surface reflectance





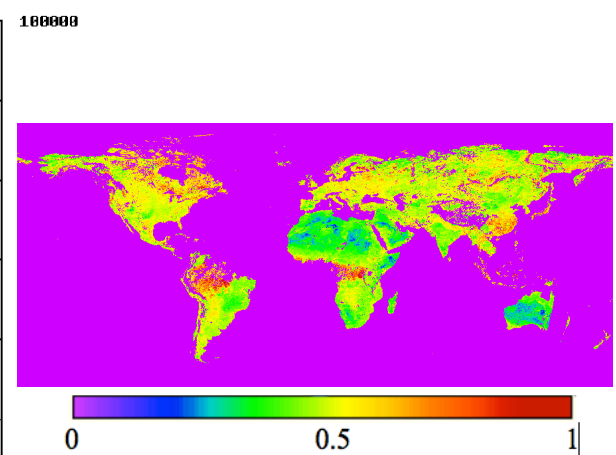
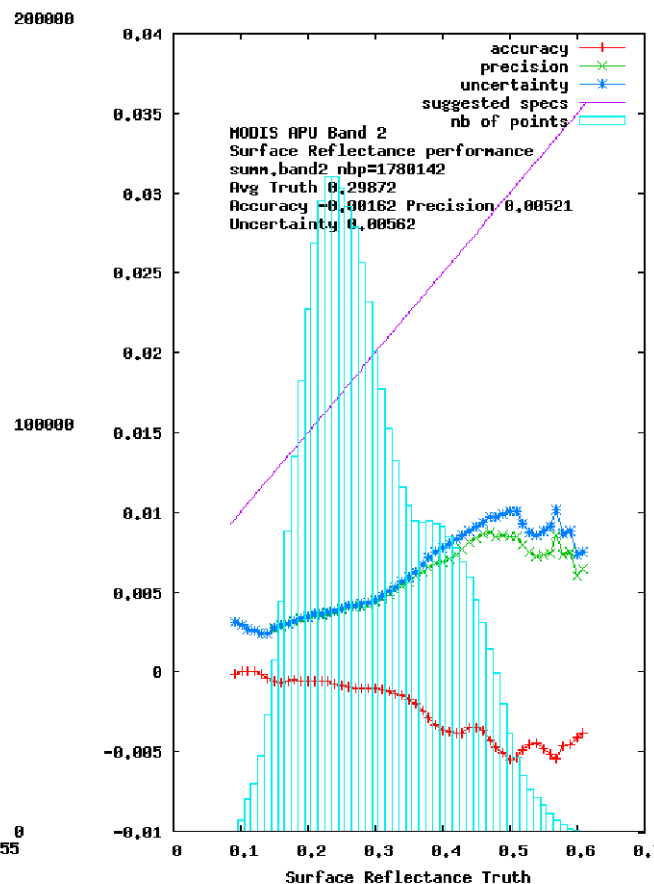
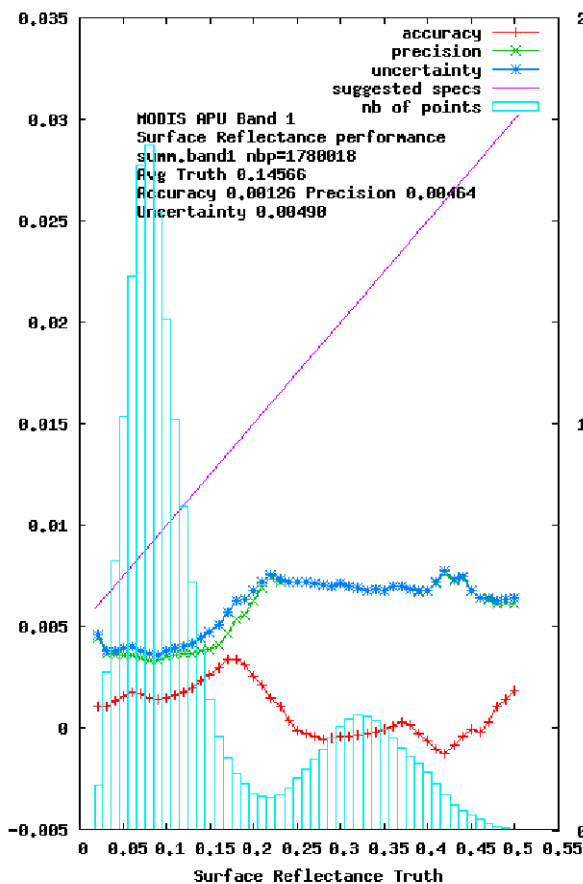
quantitative assessment of performances (APU) for MODIS (Collection 5: Fixed ratio blue/red)



COLLECTION 5: accuracy or mean bias (red line), Precision or repeatability (green line) and Uncertainty or quadratic sum of Accuracy and Precision (blue line) of the surface reflectance in band 1 in the Red (top left), band 2 in the Near Infrared (top right also shown is the uncertainty specification (the line in magenta), that was derived from the theoretical error budget. Data collected from Terra over 200 AERONET sites from 2000 to 2009.



Improving the aerosol retrieval in collection 6 reflected in APU metrics

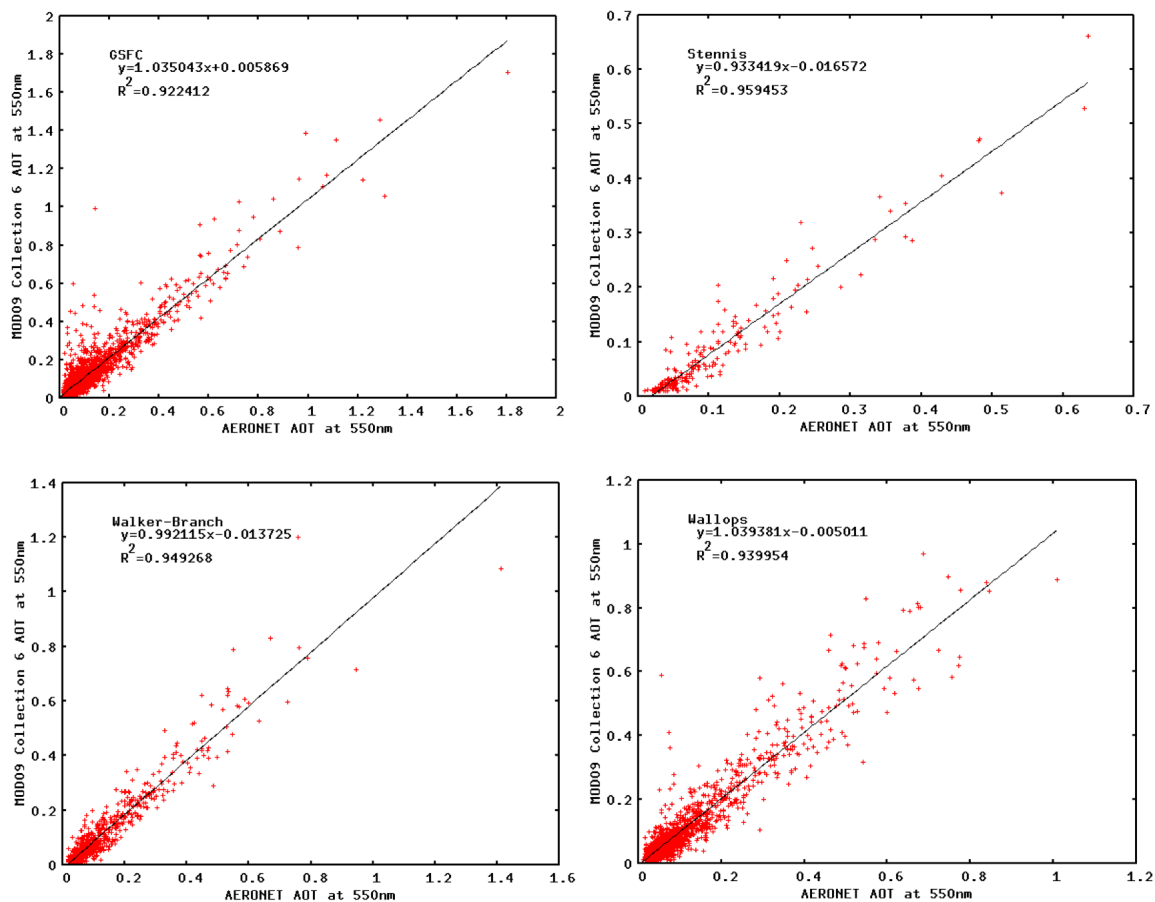


ratio blue/red derived using MODIS top of the atmosphere corrected with MISR aerosol optical depth

COLLECTION 6: accuracy or mean bias (red line), Precision or repeatability (green line) and Uncertainty or quadratic sum of Accuracy and Precision (blue line) of the surface reflectance in band 1 in the Red (top left), band 2 in the Near Infrared (top right also shown is the uncertainty specification (the line in magenta), that was derived from the theoretical error budget. Data collected from Terra over 200 AERONET sites for the whole Terra mission.



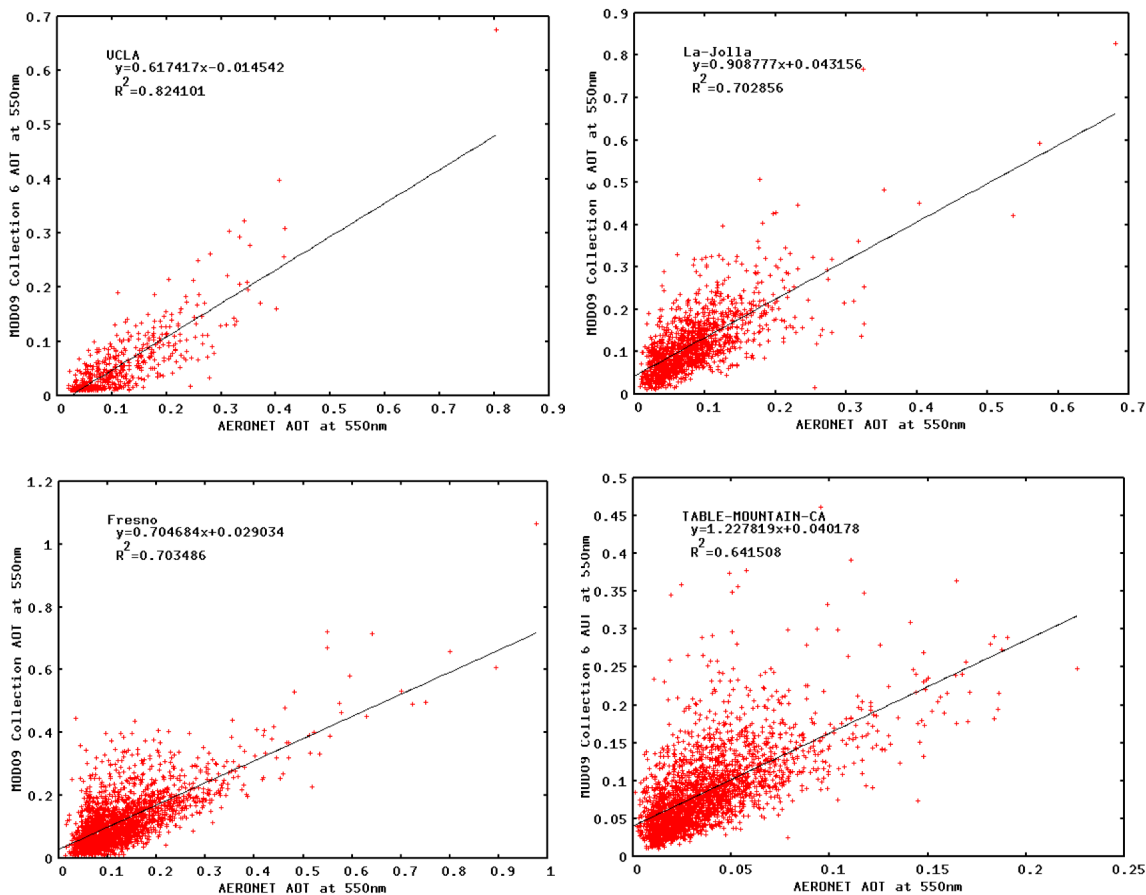
Aerosol retrieval also shows improvement



Scatterplot of the MOD09 AOT at 550nm versus the AERONET measured AOT at 550nm for East Coast sites selection: GSFC (top left), Stennis (top right), Walker Branch (bottom left) and Wallops (bottom right).



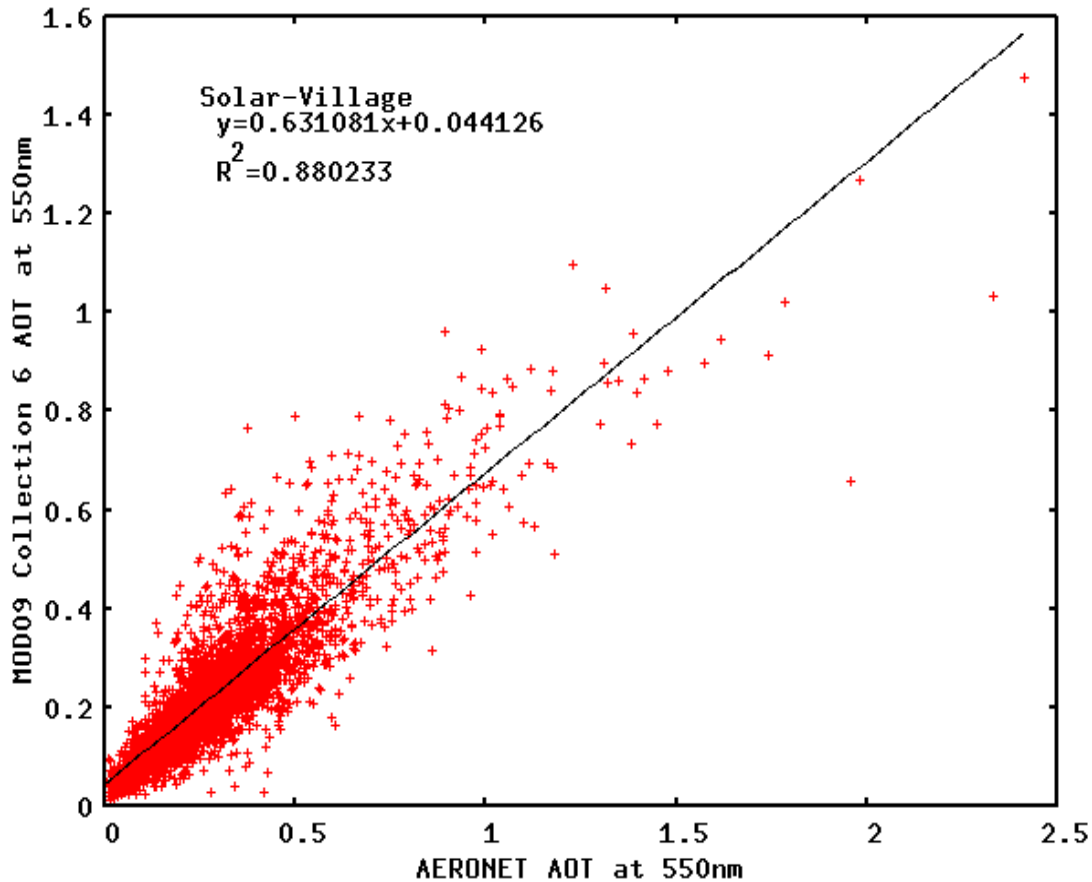
Aerosol retrieval also shows improvement



Scatterplot of the MOD09 AOT at 550nm versus the AERONET measured AOT at 550nm for the West Coast sites selection: UCLA (top left), La Jolla (top right), and Fresno (bottom left) and Table Mountain (bottom right).



Aerosol retrieval also shows improvement



Scatterplot of the MOD09 AOT at 550nm versus the AERONET measured AOT at 550nm for for a very bright site in Saudi Arabia (Solar Village)



Landsat8/OLI and Sentinel 2/MSI Surface Reflectance is largely based on MODIS C6 (LaSRC)

Algorithm reference for L8: Vermote E., Justice C., Claverie M., Franch B., (2016) "Preliminary analysis of the performance of the Landsat 8/OLI land surface reflectance product", Remote Sensing of Environment, 185,46-56.

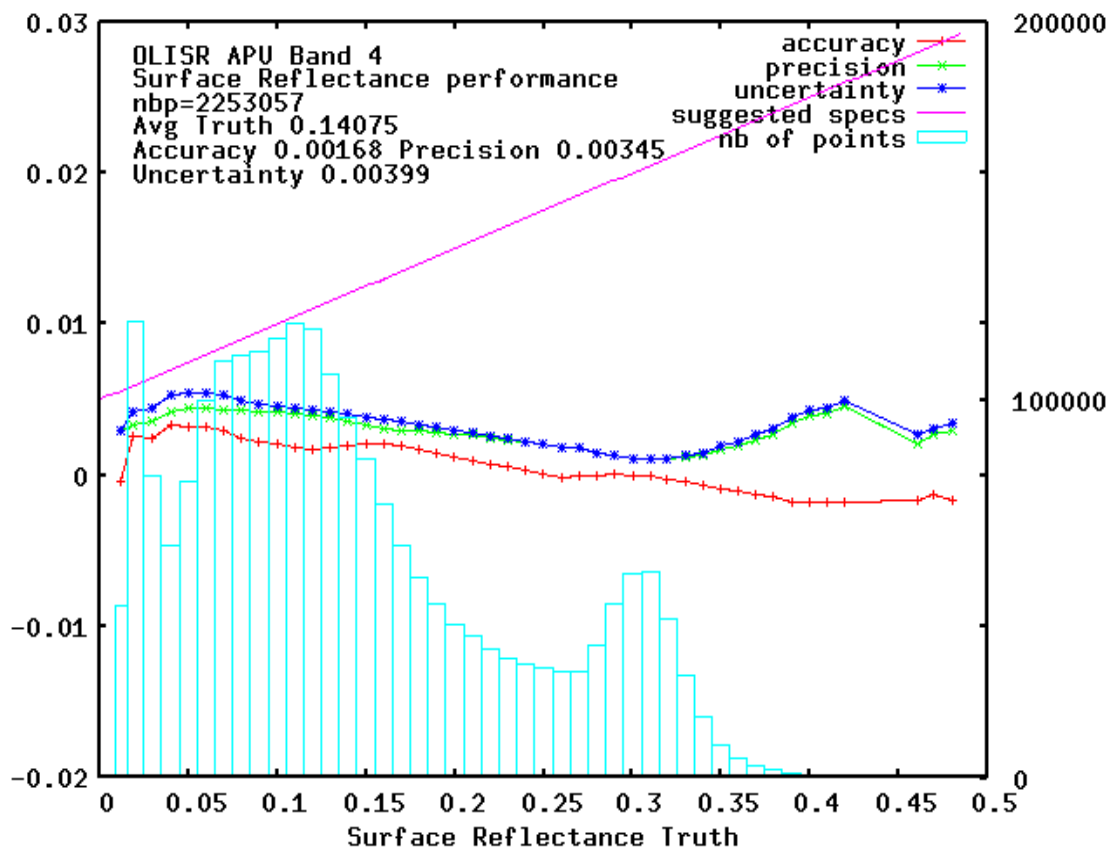
The MODIS **Collection 6 AC algorithm** relies on

- the use of very accurate (better than 1%) vector radiative transfer modeling of the coupled atmosphere-surface system (6S)
- the inversion of key atmospheric parameters
 - ***Aerosols are retrieved from Landsat8/Sentinel 2 images***
 - ***Water vapor and ozone from daily MODIS product.***

Home page: <http://modis-sr.ltdri.org>



Evaluation of the performance of Landsat8



The “preliminary” analysis of OLI SR performance in the red band over AERONET is very similar to MODIS Collection 6



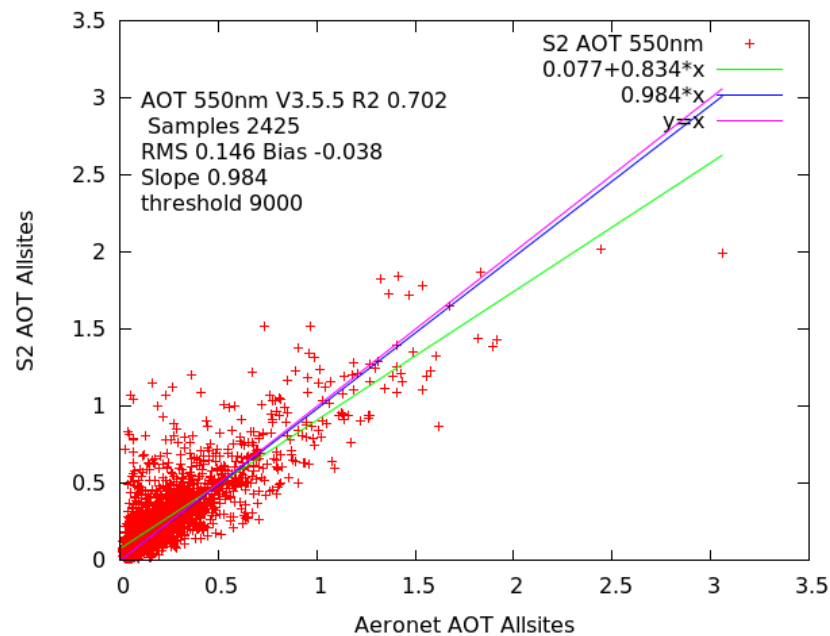
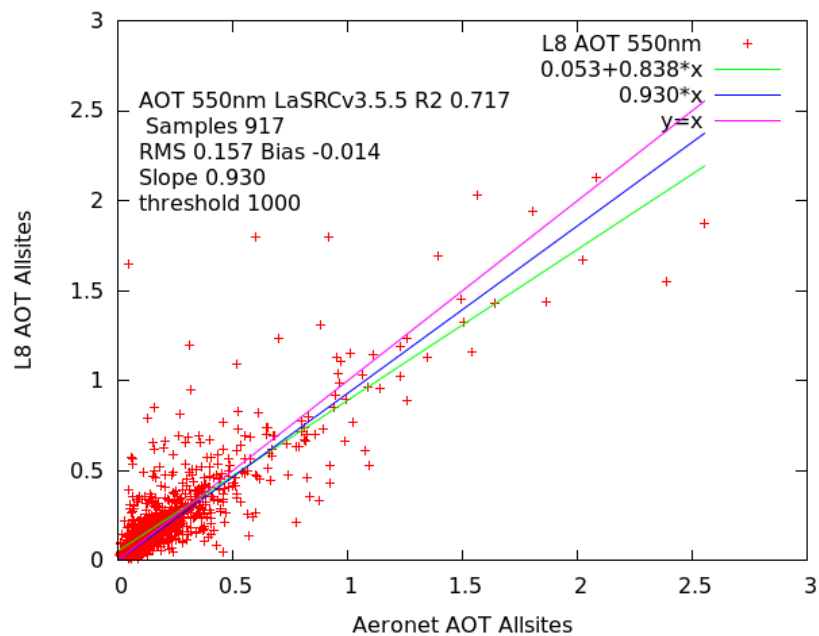
This is confirmed by comparison with MODIS

OLI Band	TM LEDAPS (Claverie et al., 2015)			ETM+ LEDAPS (Claverie et al., 2015)			OLI (Vermote et al., 2016)		
	A	P	U	A	P	U	A	P	U
2	7	9	11	9	7	12	2	6	6
3	1	9	9	6	9	11	3	6	7
4	9	10	14	1	9	9	1	6	6
5	5	17	17	3	14	15	2	12	12
7	1	14	14	5	15	16	9	11	14

OLI surface reflectance APU scores expressed in 10^{-3} reflectance (compared to TM and ETM+ surface reflectance APU by Claverie et al. (2015) using Aqua MODIS BRDF and spectrally adjusted surface reflectance CMG product as reference, the OLI surface reflectance was aggregated over the CMG. Band number corresponds to OLI band number designation and equivalent TM/ETM+ bands were reported.

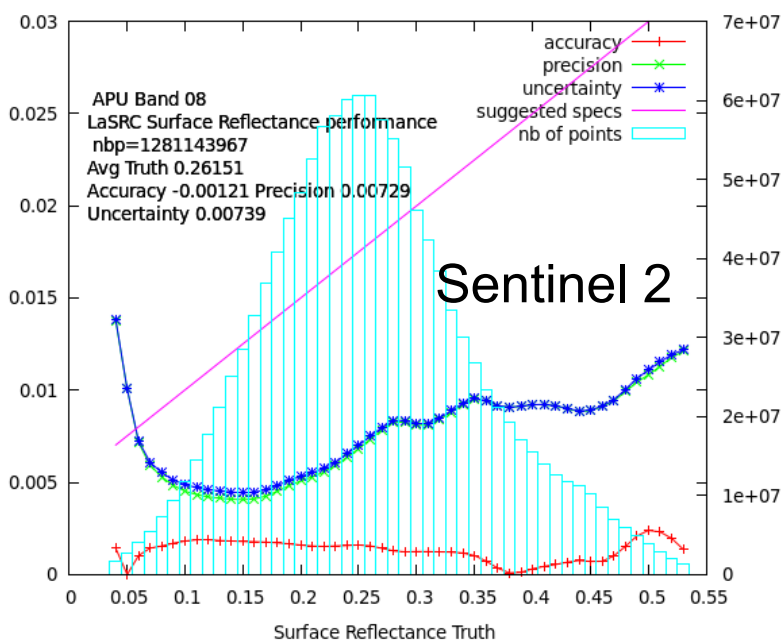
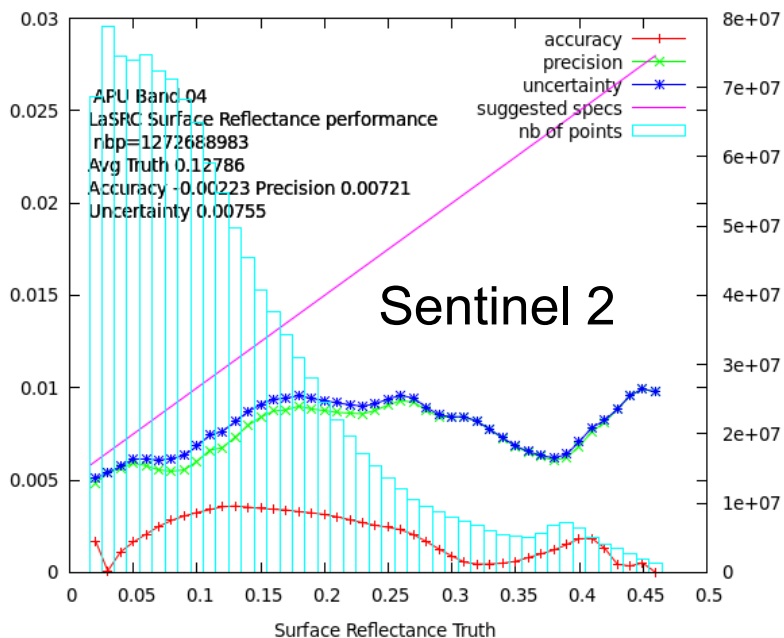
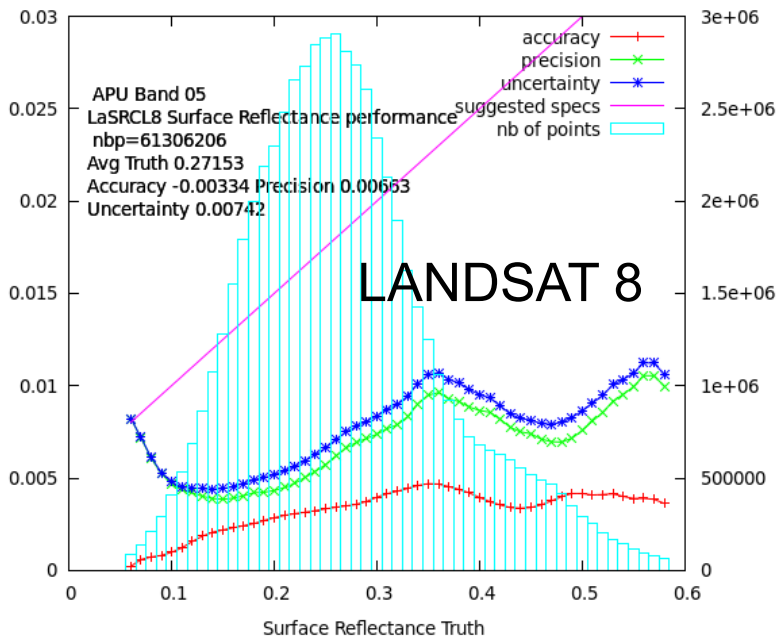
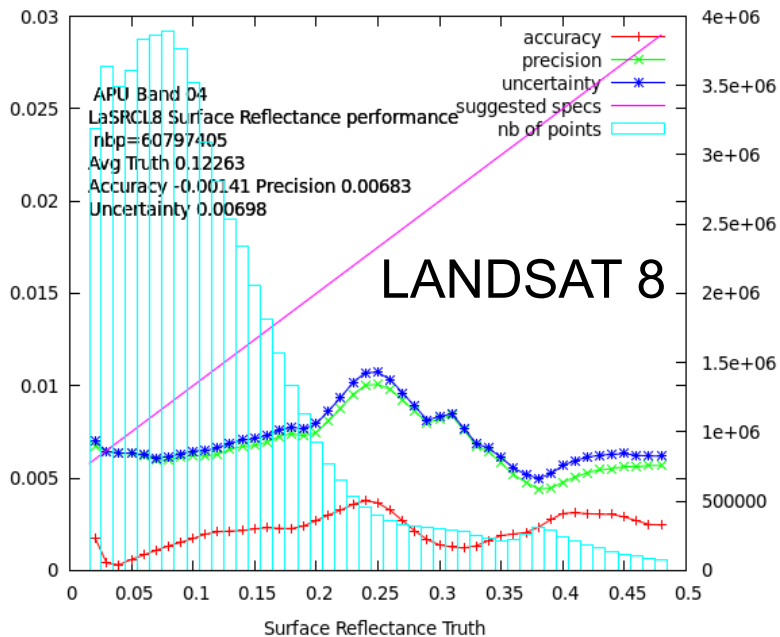


LaSRC AOT Results on ACIX-II





LaSRC APU results on ACIX-II





Performances on AOD retrieval over urban environment

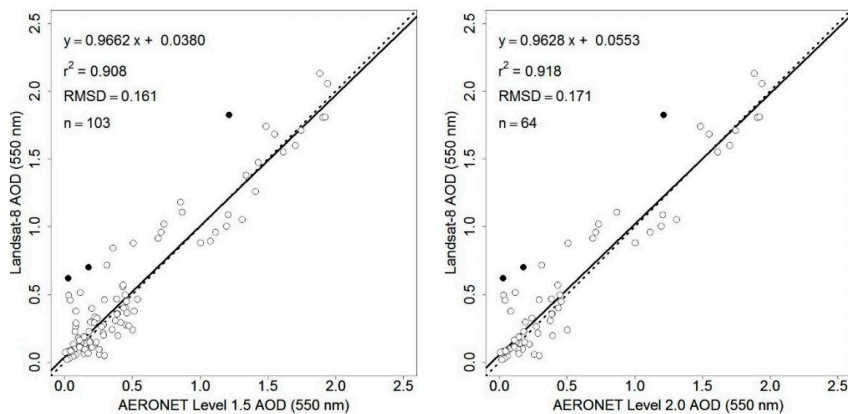


Figure 3. Scatterplots of the Landsat-8 AOD against the contemporaneous AERONET Level 1.5 (left) and Level 2.0 (right) AOD data over the urban AERONET sites for 2016. The three filled circles are outliers due to Landsat-8 cloud detection omission errors and are not used in statistics analysis. The solid lines show ordinary least square regression lines. The dotted lines are 1:1 lines superimposed for reference.

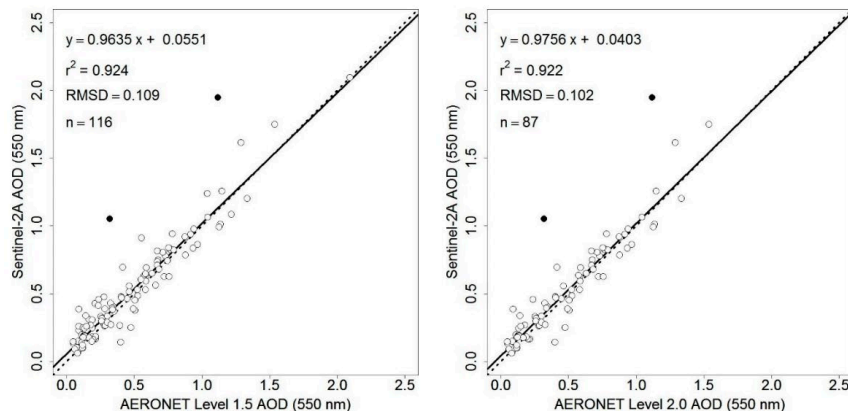
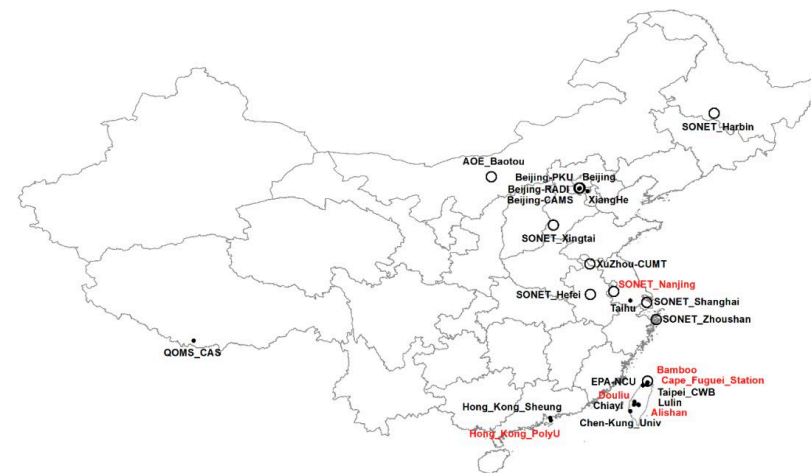


Figure 4. Scatterplots of the Sentinel-2A AOD against the contemporaneous AERONET Level 1.5 (left) and Level 2.0 (right) AOD data over the urban AERONET sites for 2016. The two filled circles are outliers due to Sentinel-2A cloud detection omission errors and are not used in statistics analysis. The solid lines show ordinary least square regression lines. The dotted lines are 1:1 lines superimposed for reference.

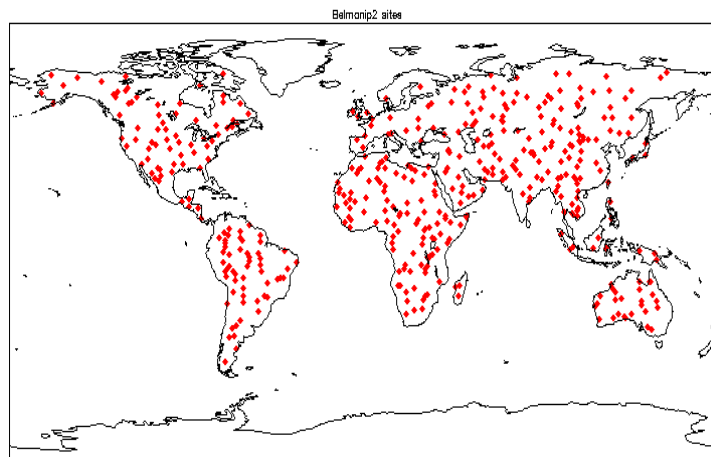
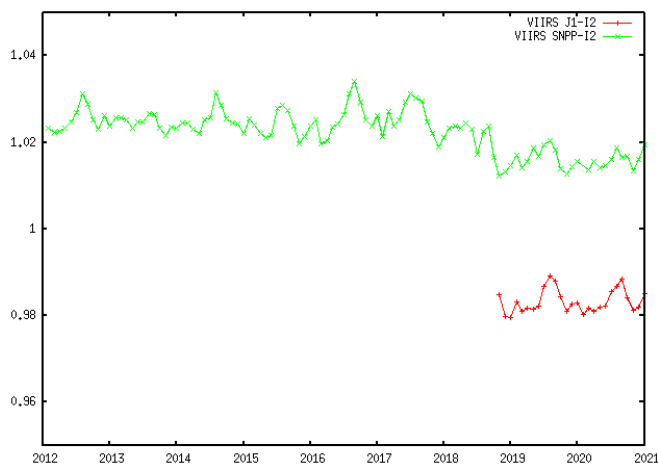
Li, Z., Roy, D. P., Zhang, H. K., Vermote, E. F., & Huang, H. (2019). Evaluation of Landsat-8 and Sentinel-2A aerosol optical depth retrievals across Chinese cities and implications for medium spatial resolution urban aerosol monitoring. *Remote sensing*, 11(2), 122.





Datasets for S3 evaluation

- MODIS Terra, Aqua, S3 (CMG) over Belmanip sites (422) during December 2018.
- Data were corrected for BRDF and normalize to Nadir view sun at 45deg.

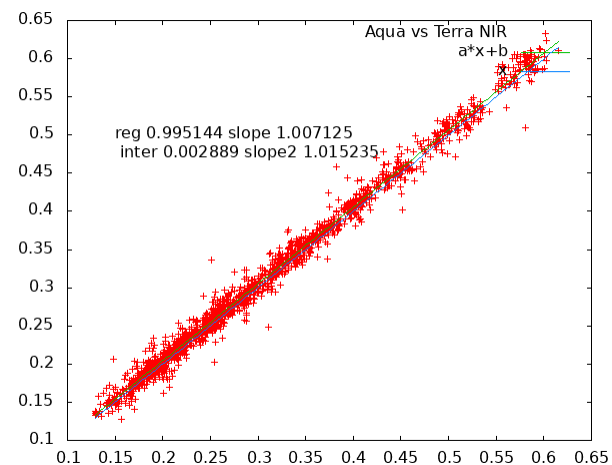
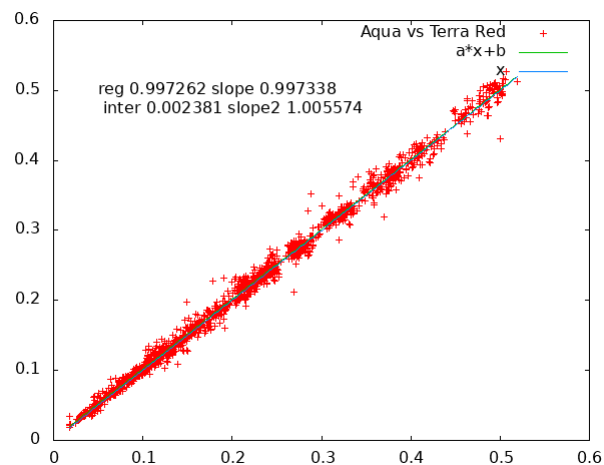
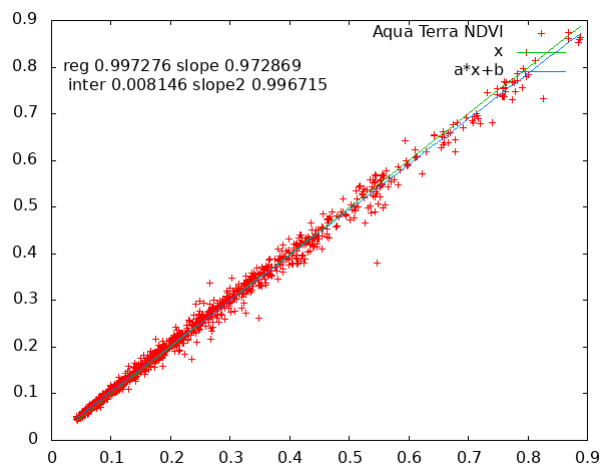


Automated monthly VIIRS cross comparison (over BELMANIP sites) with MODIS Aqua from 2012. the stability of both VIIRS and MODIS Aqua is excellent in both red and NIR as shown ($\pm 0.5\%$).



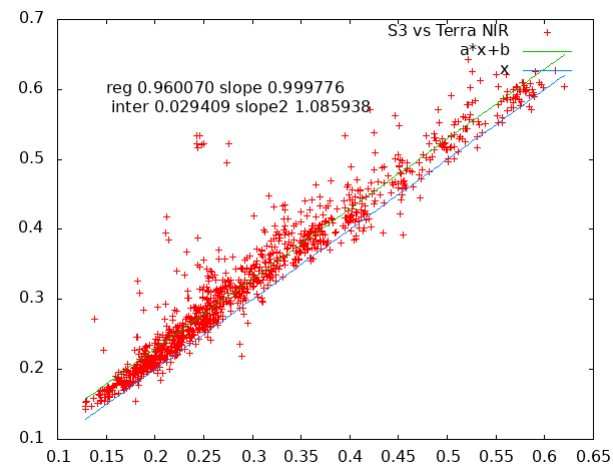
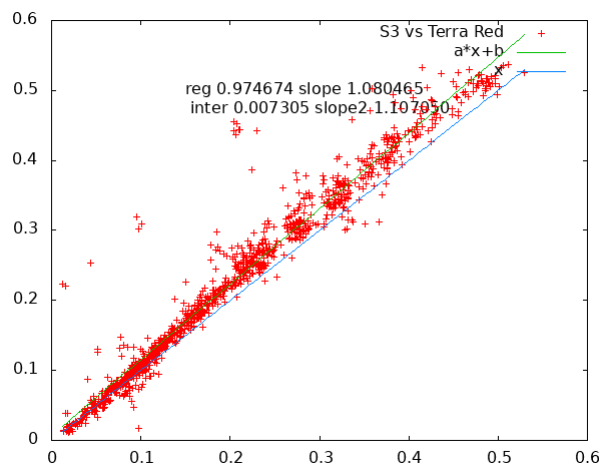
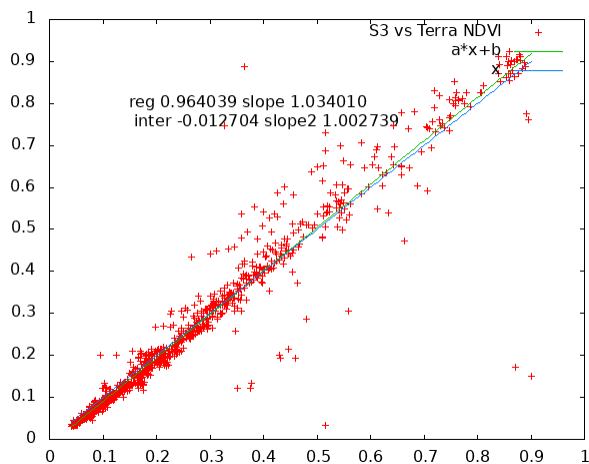
Scatters plot : Aqua vs Terra

Dec 2018



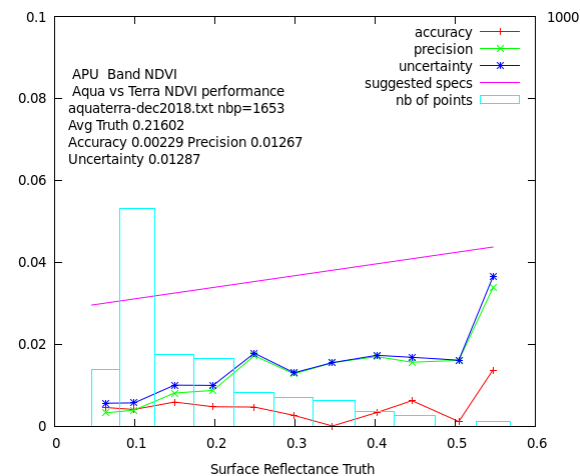
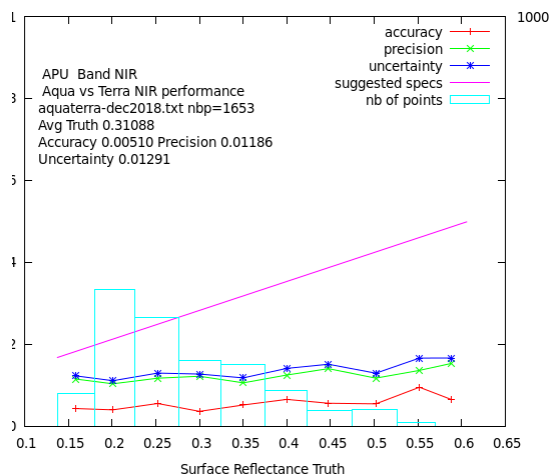
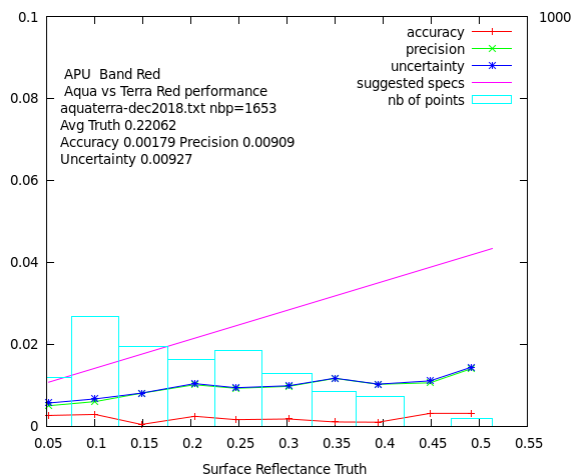


Scatters plot : S3 vs Terra Dec 2018



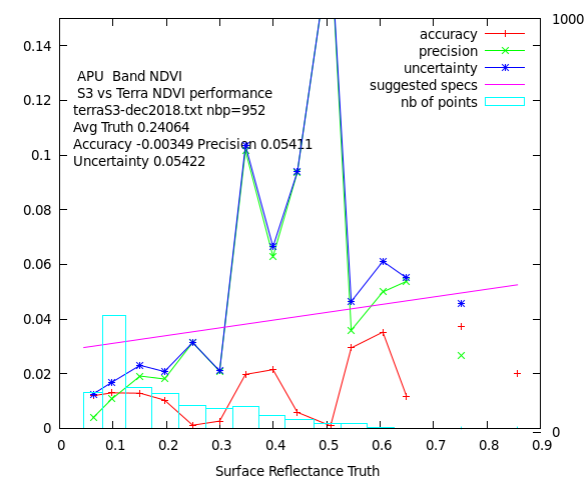
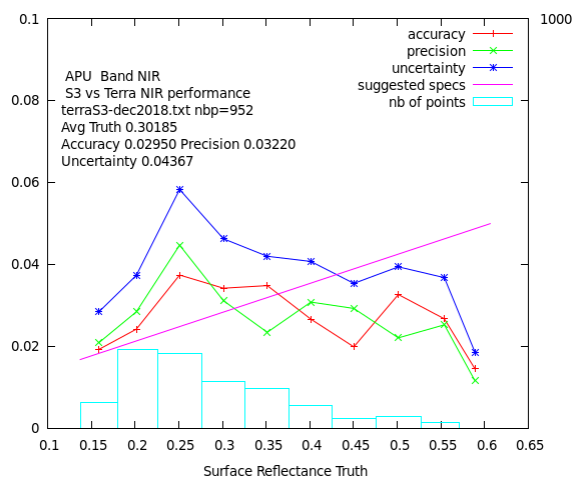
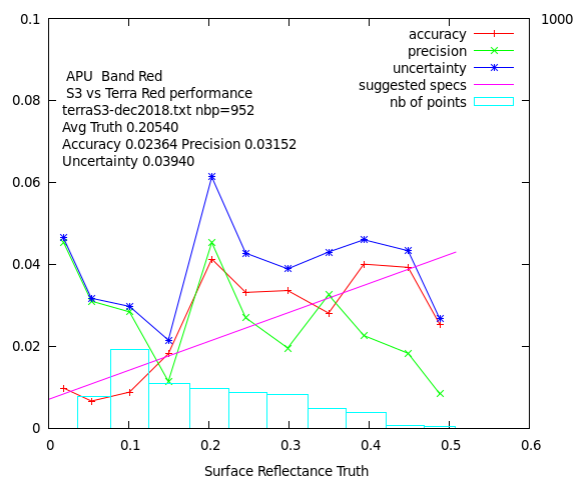


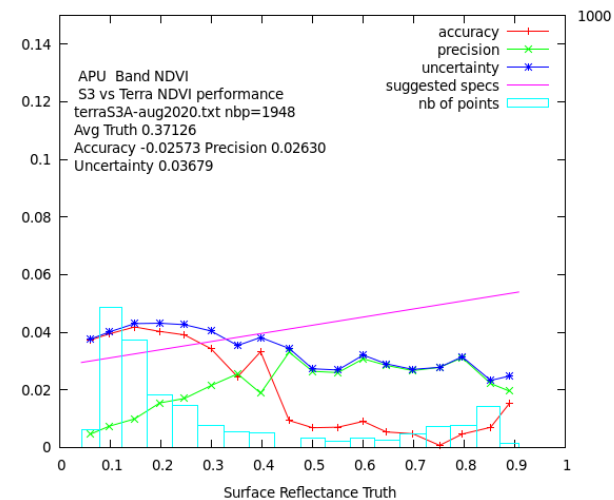
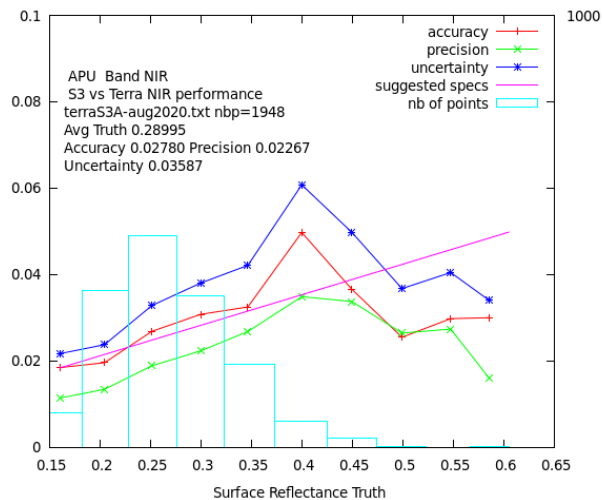
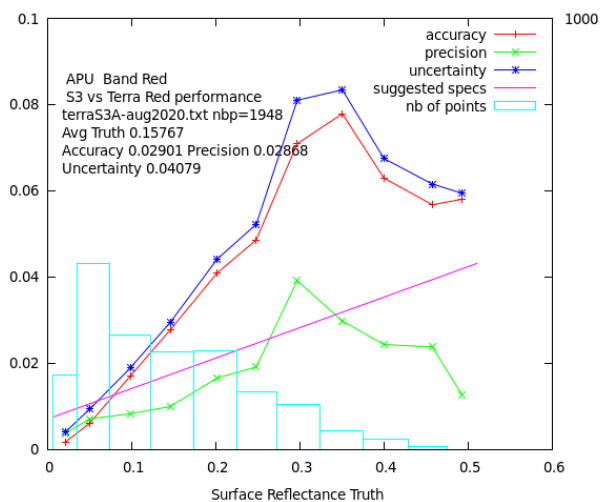
APU: Aqua vs Terra Dec 2018



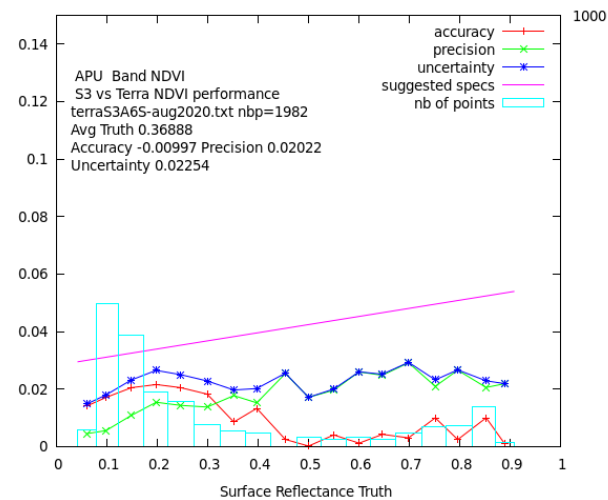
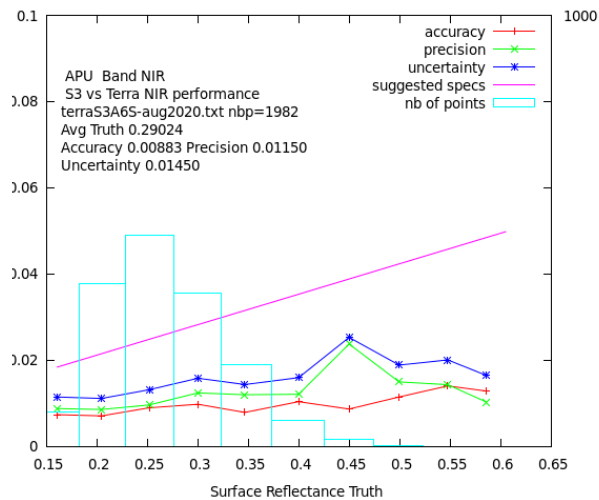
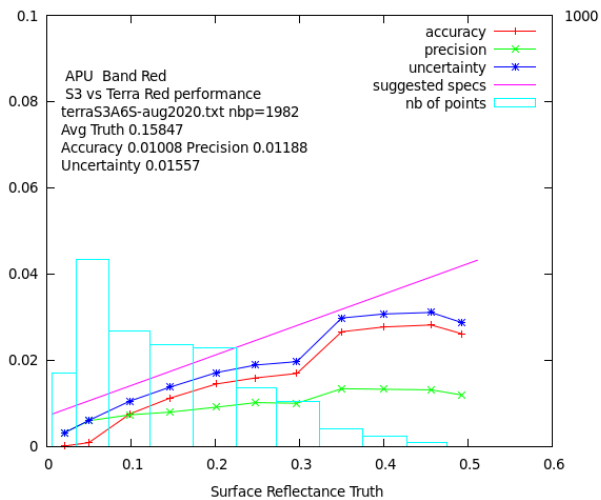


APU: S3 vs Terra Dec 2018





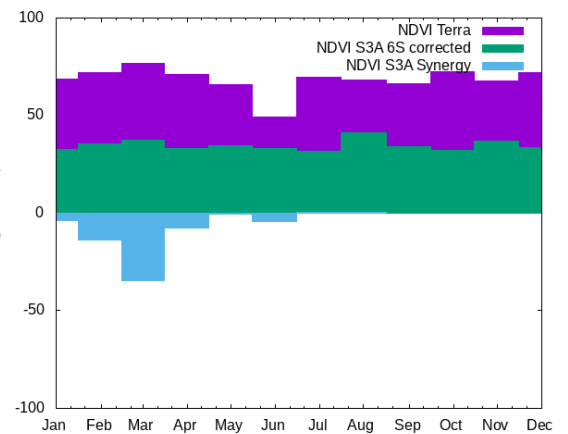
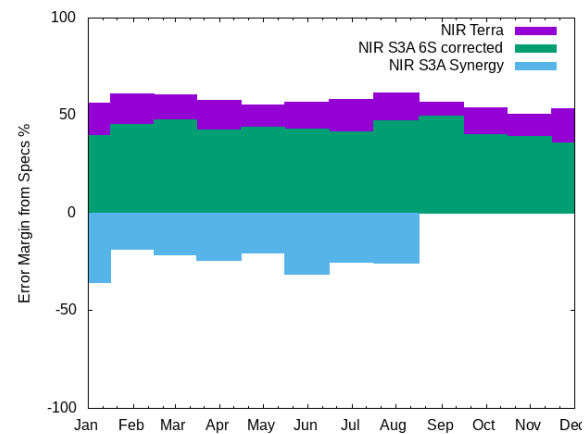
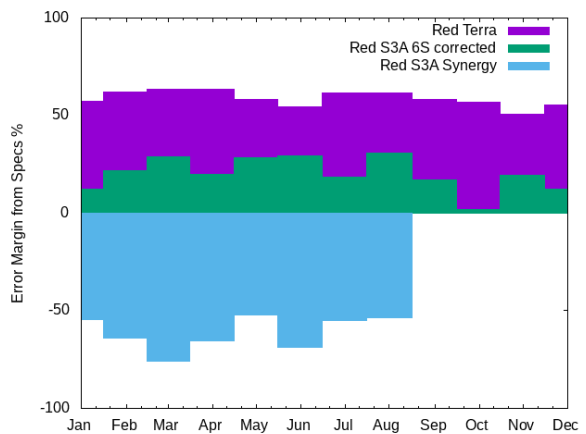
Sentinel 3 SR versus Terra (APU) Aug 2020



Sentinel 3 6S-SR versus Terra (APU) Aug 2020

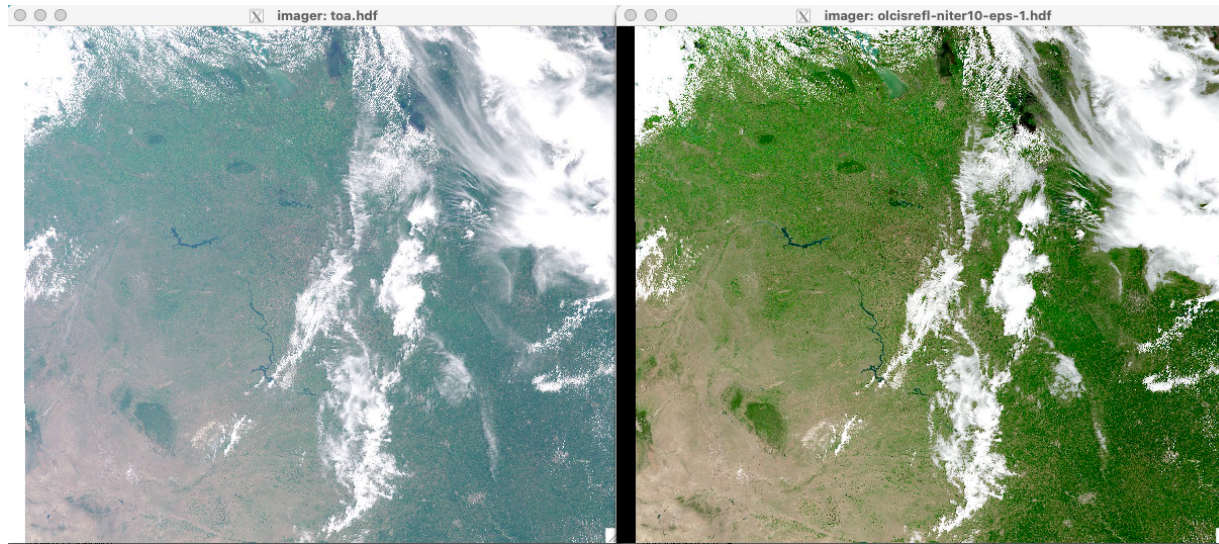


Summary performances for 2020 (Uncertainty)





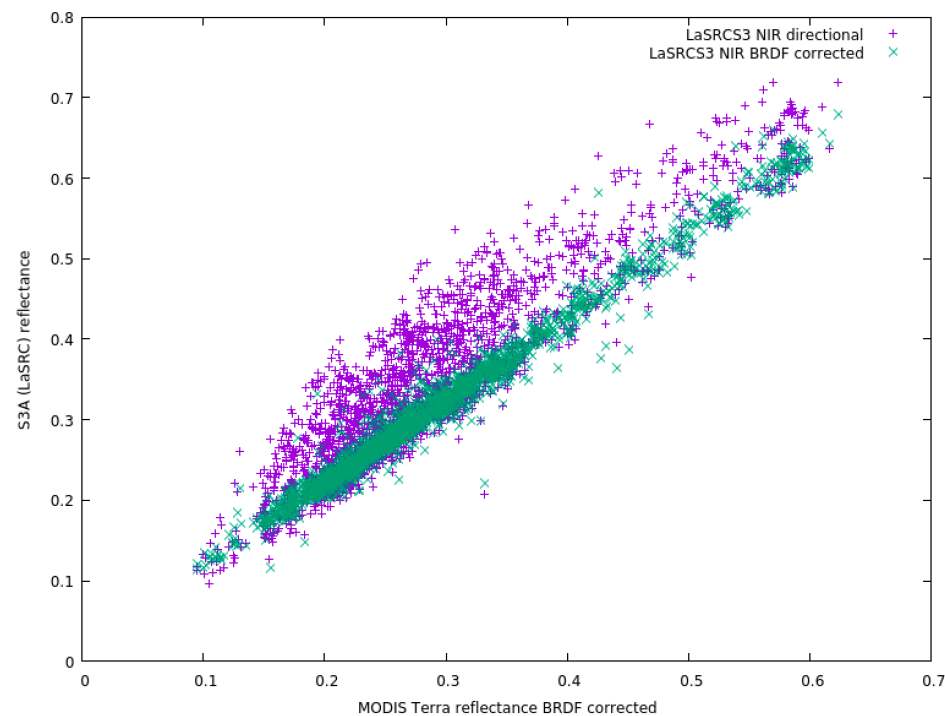
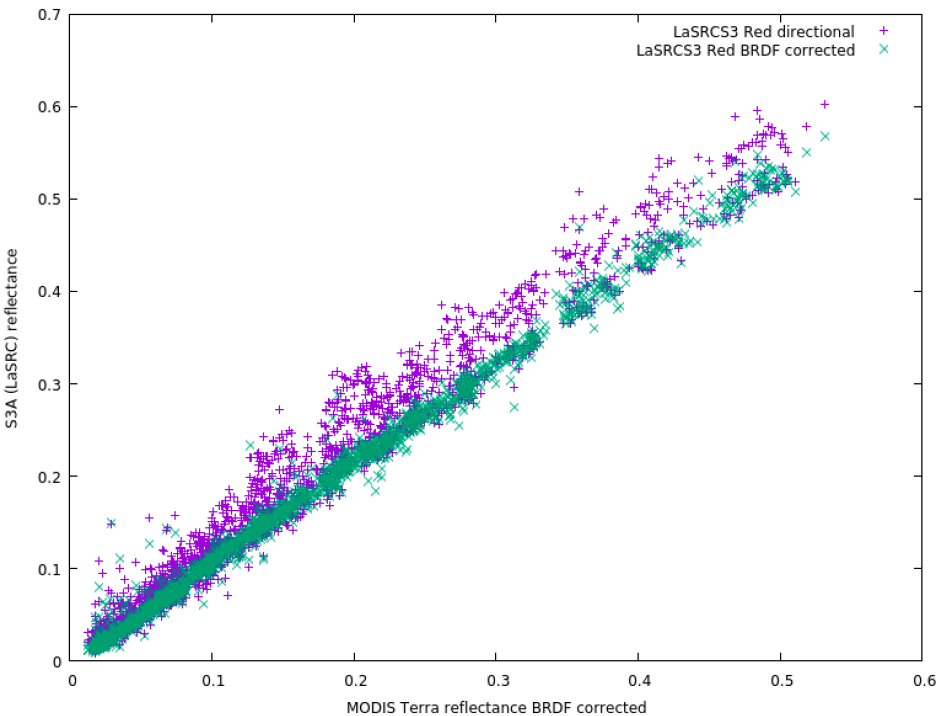
LaSRC Prototype for S3-OLCI – First results



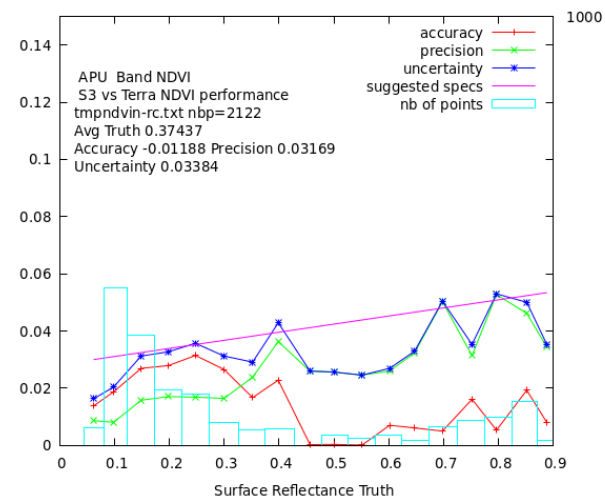
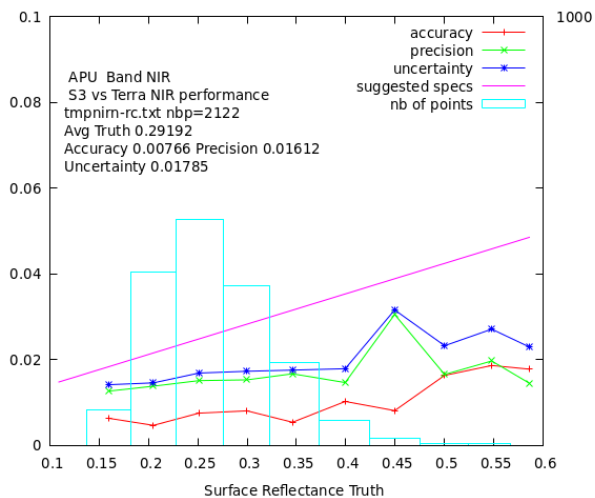
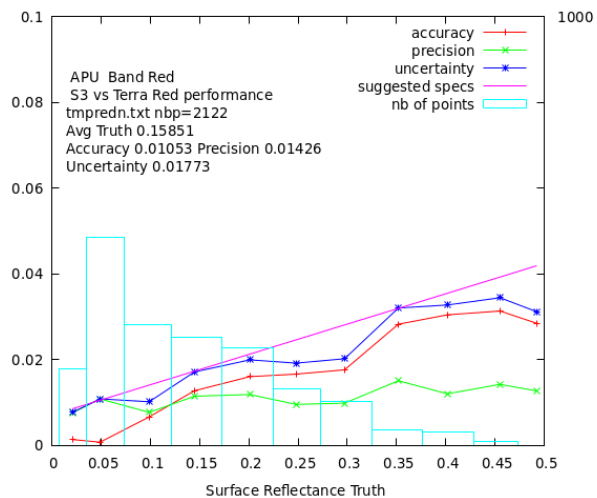
OLCI TOA Reflectance (RGB) OLCI LaSRC Surface Reflectance (RGB)



LaSRC Prototype for S3-OLCI – First results



Comparison over BELMANIP2 sites for August 2020



Sentinel 3 LaSRC-SR versus Terra (APU) Aug 2020



Cloud validation: SkyCam

- Ground-based skycam
 - For objective validation of satellite-derived cloud masks
 - Proof of concept: manual iphone with fisheye lens over NASA GSFC
 - Current version: automatic, enabling replication over multiple sites
 - Part of validation dataset within CEOS CMIX-1 (Cloud Masking Inter-comparison Exercise)

International Journal of Applied Earth Observations and Geoinformation 95 (2021) 102253



An experimental sky-image-derived cloud validation dataset for Sentinel-2 and Landsat 8 satellites over NASA GSFC

Sergii Skakun^{a,b,c,*}, Eric F. Vermote^c, Andres Eduardo Santamaria Artigas^{a,c}, William H. Rountree^{a,c}, Jean-Claude Roger^{a,c}

^a Department of Geographical Sciences, University of Maryland, College Park, MD 20742, USA
^b College of Information Studies (School), University of Maryland, College Park, MD 20742, USA
^c NASA Goddard Space Flight Center Code 619, 8800 Greenbelt Road, Greenbelt, MD 20771, USA

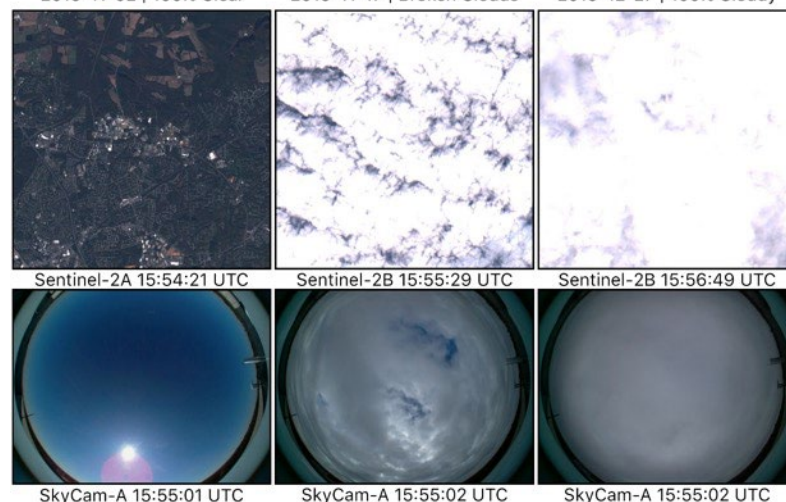
Satellite image (true color)

Satellite image (cirrus band)

Ground-based image of the sky



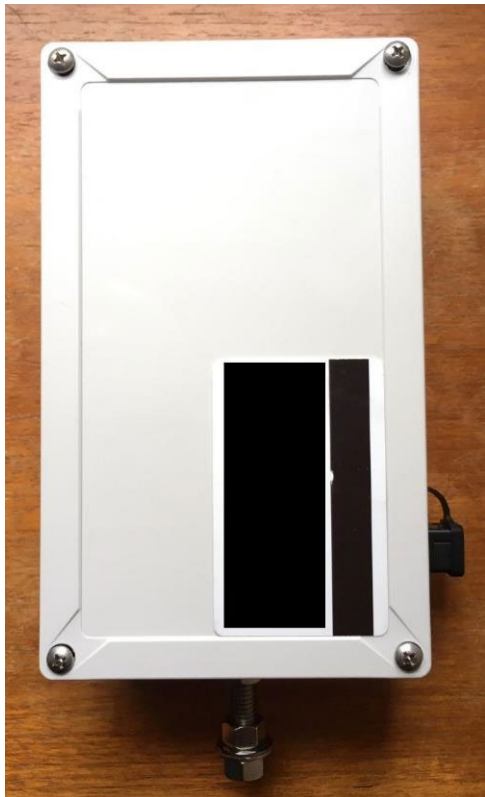
2019-11-02 | 100% Clear 2019-11-17 | Broken Clouds 2019-12-27 | 100% Cloudy





12 cm

20 cm



Self-contained system:

RGB camera

~180-degree lens

Single board computer (Raspberry-Pi)

Power delivery (POE/Alternatives)

Weatherproof* enclosure (IP66/IP67)

Weight ~750g per unit.



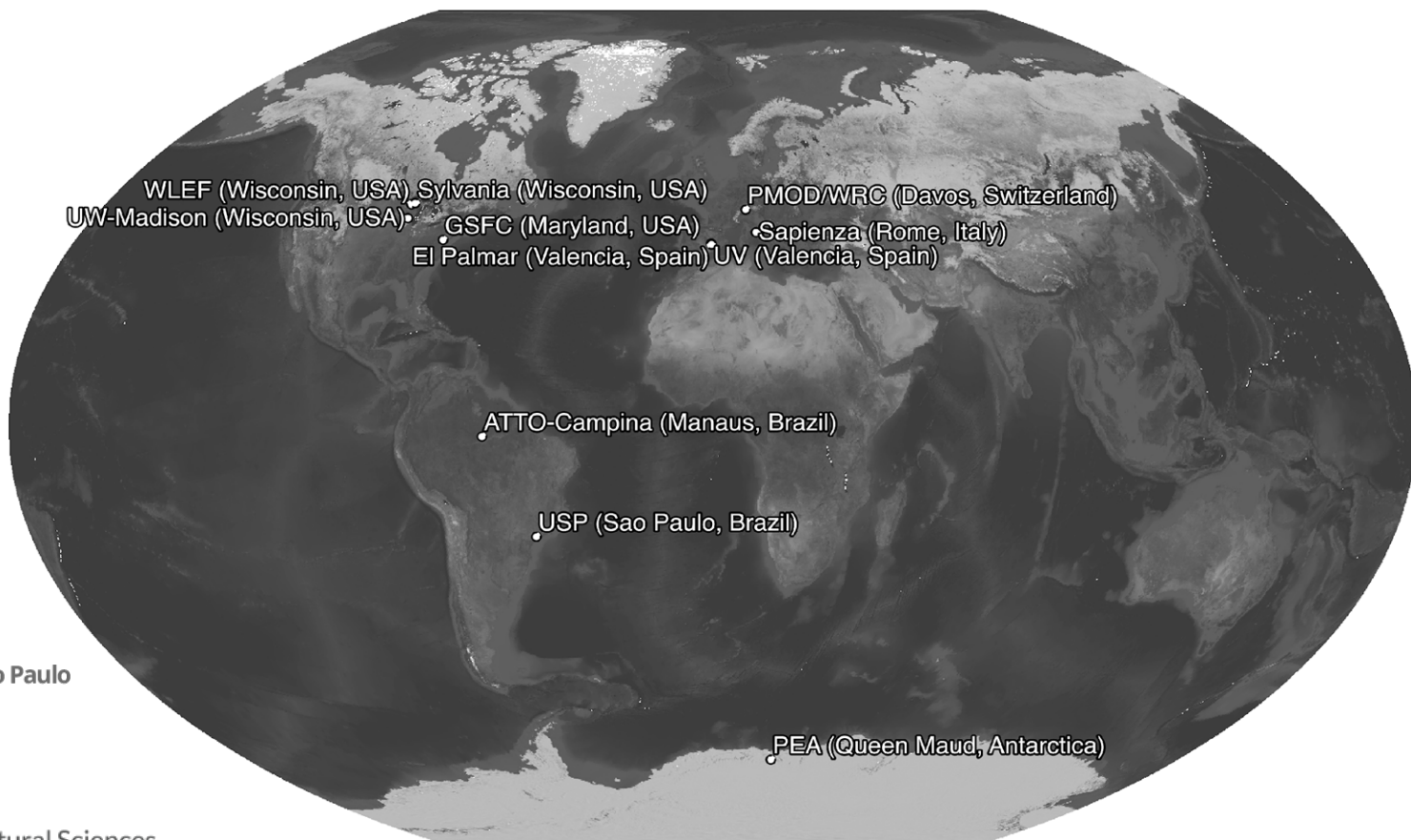
7.5 cm



VNIVERSITAT
D VALÈNCIA

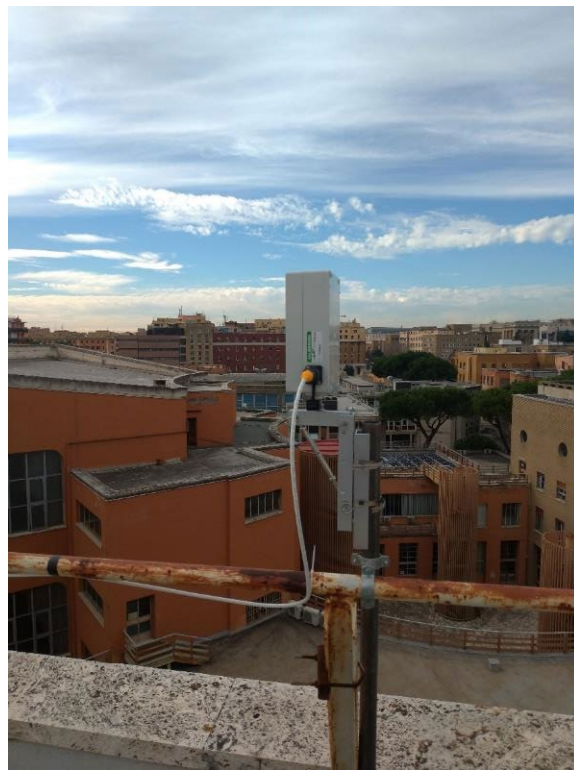


pmod) *wrc*





SKYCAM1 at GSFC Building 33
Maryland, USA



SKYCAM2 at U. Sapienza Physics Dept.
Rome, Italy



SKYCAM2 at U. Valencia Physics Dept.
Valencia, Spain



SKYCAM1 at PEA
Queen Maud, Antarctica



SKYCAM2 at El Palmar
Valencia, Spain

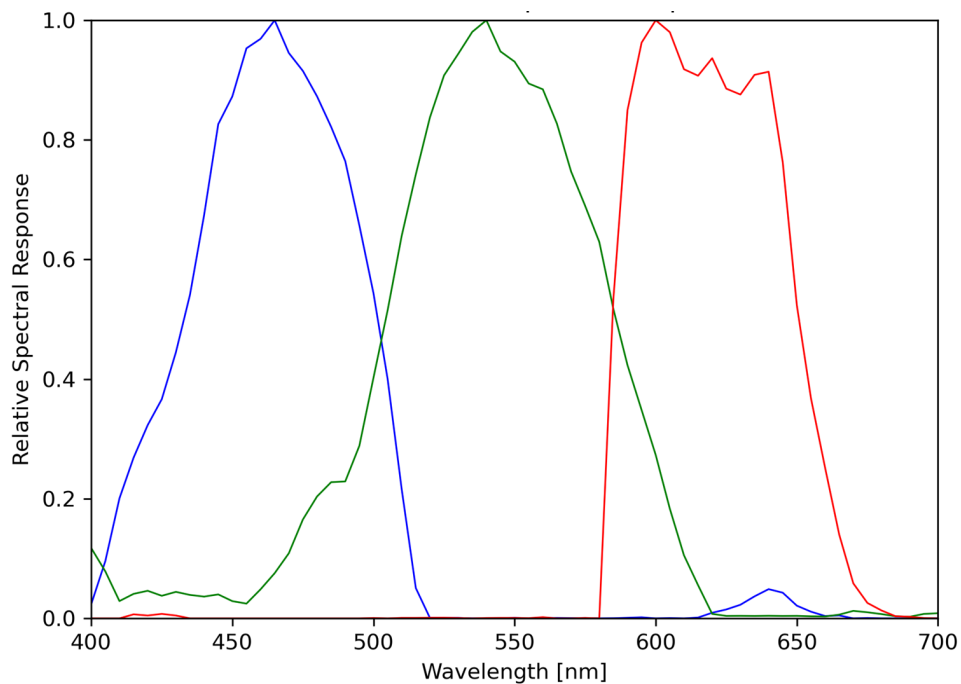


SKYCAM1 at PMOD/WRC
Davos, Switzerland



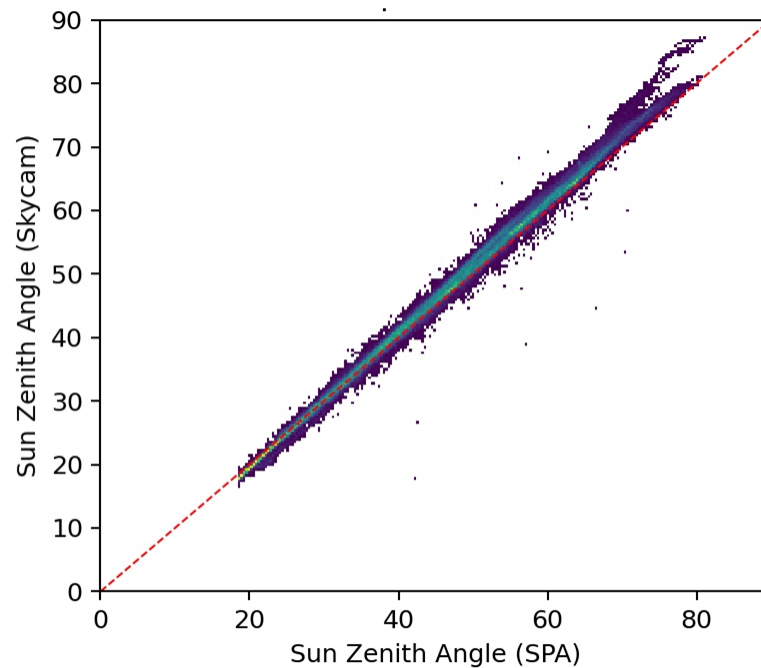
SKYCAM Characterization

SKYCAM Relative Spectral Response¹



¹Measured at GSFC Code 618 using Digikröm DK240 Monochromator and ASD Fieldspec Spectroradiometer

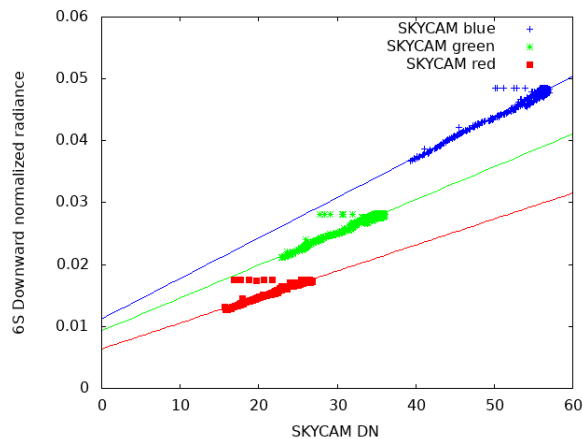
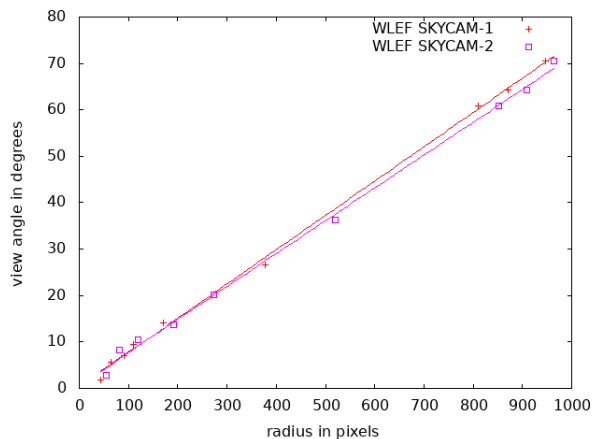
Sun Zenith Angle
SKYCAM estimation vs NREL SPA²



²US National Renewable Energy Laboratory Solar Position Algorithm



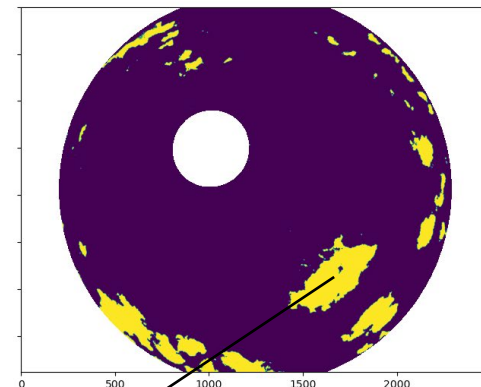
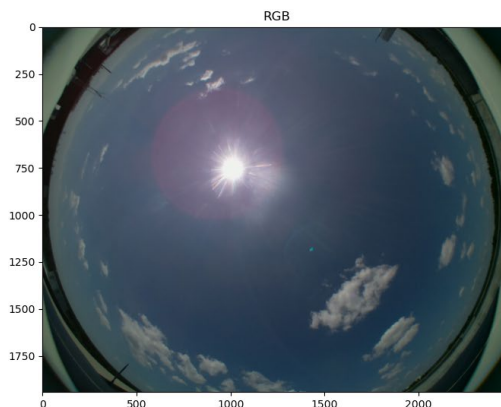
SKYCAM Calibration (geometric/radiometric)



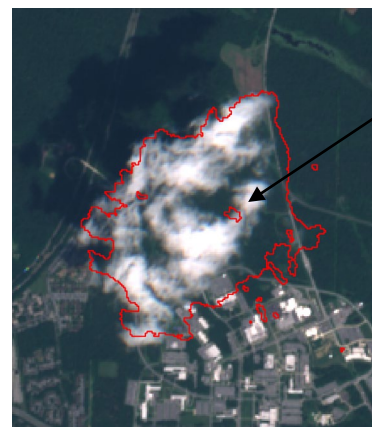


From Sky Camera to Satellite Cloud Mask

- Classification of cloud/non-cloud
 - MLP model based on a database of fully cloudy and cloud-free images
- Reprojection to satellite geometry
 - Requires cloud height
- Refining the cloud mask



Classification: cloud/non-cloud



Automatic projection from skycam geometry to satellite

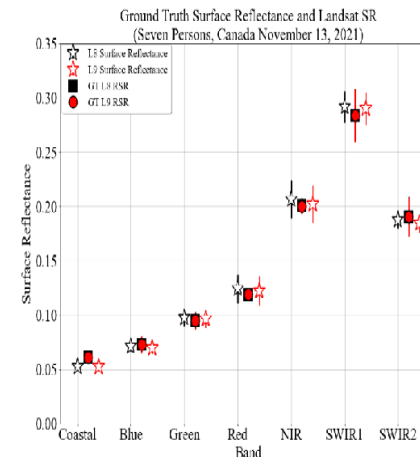
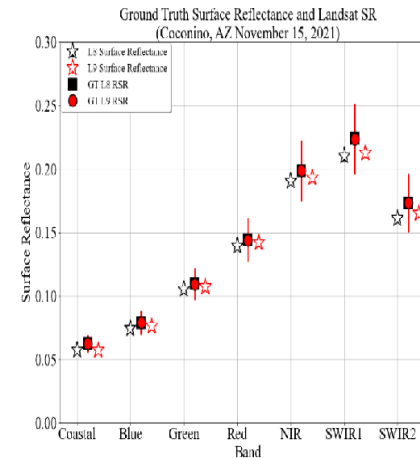


Refined cloud mask

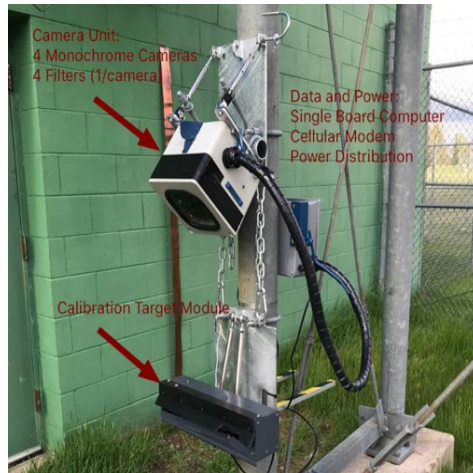


Ground Validation using episodic ground measurements over uniform/stable/arid sites

Ratio of L9 and L8 Surface Reflectance Products					
Band	Guymon (ECCOE)	Coconino (ECCOE)	Ivanpah Playa (UArizona)	Seven Persons (U of Lethbridge)	Wilcannia (GA)
Coastal/Aerosol	0.995	0.999	0.97	0.996	1.005
Blue	0.980	1.023	0.99	0.974	1.001
Green	0.987	1.015	1.01	0.991	1.002
Red	0.991	1.019	1.00	0.986	0.998
NIR	0.999	1.014	0.98	0.979	1.001
SWIR1	0.995	1.011	1.02	0.994	1.007
SWIR2	0.989	1.026	1.03	0.982	0.994



Ground Validation using CAMSIS



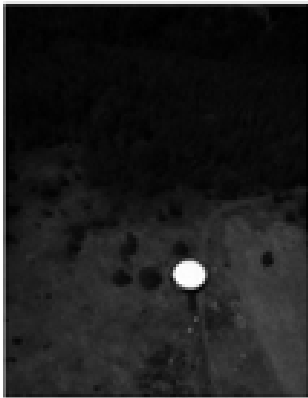
CAMSIS system



CAMSIS is installed at a height of 123m on a TV tower (WLEF) near Park Falls, WI at the Chequamegon National Forest

CAMSIS Data processing

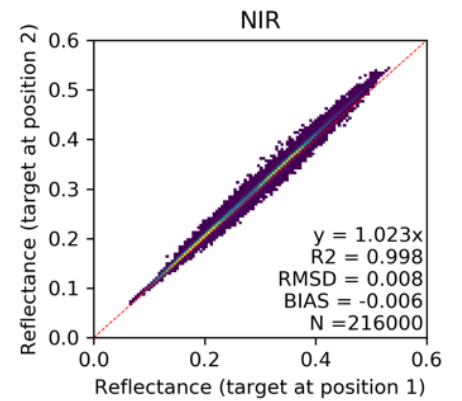
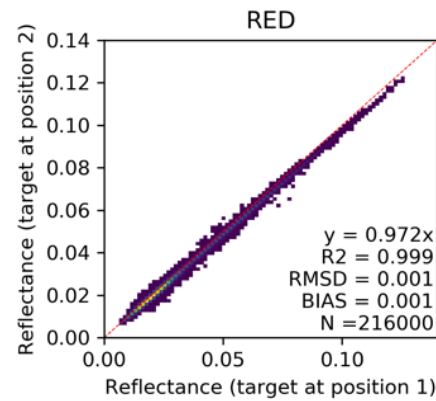
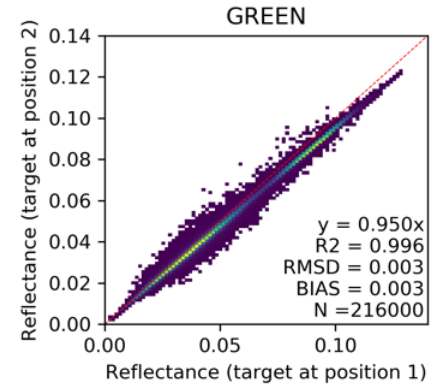
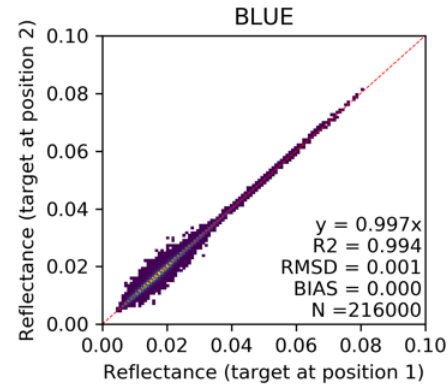
Raw 1



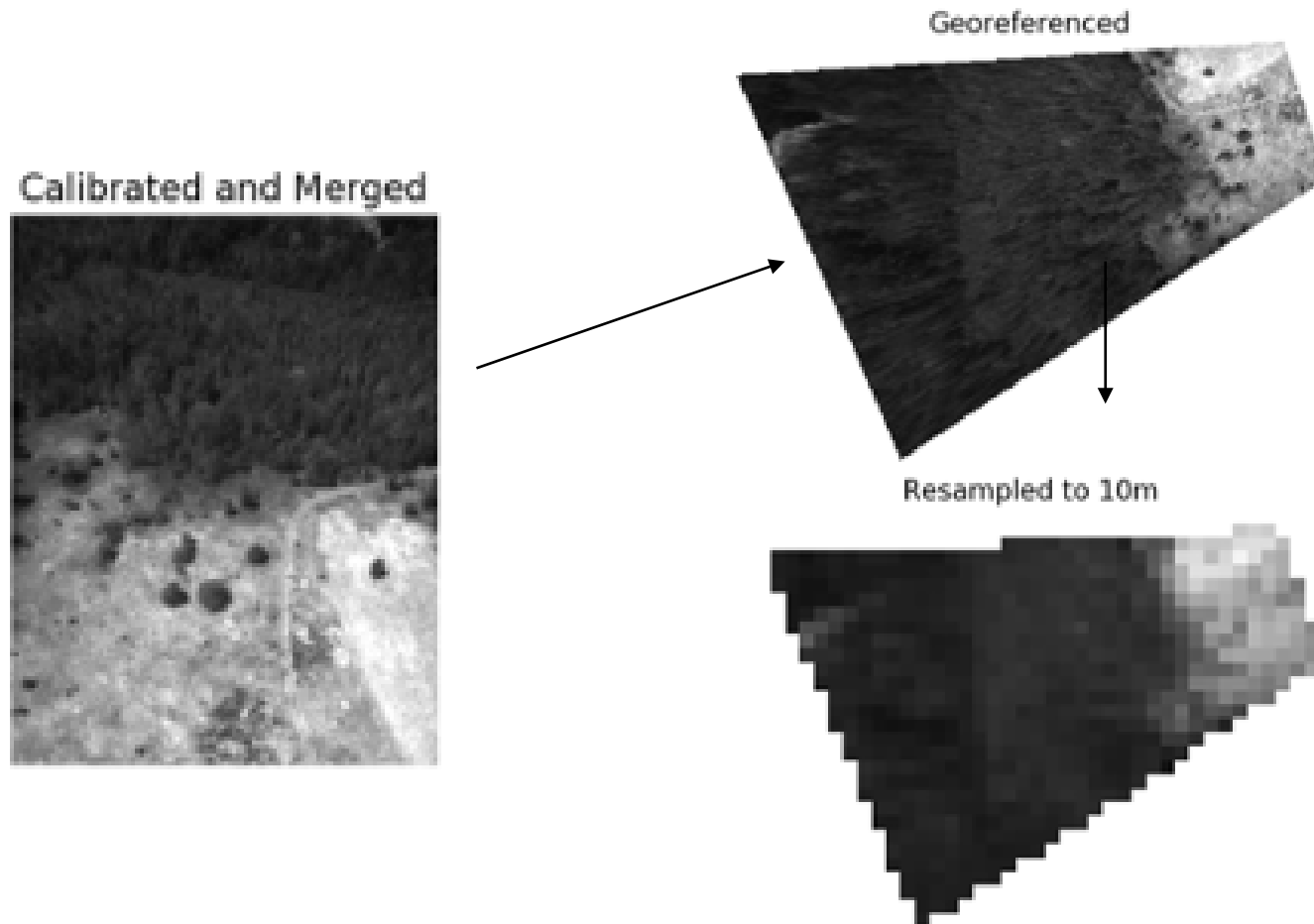
Raw 2



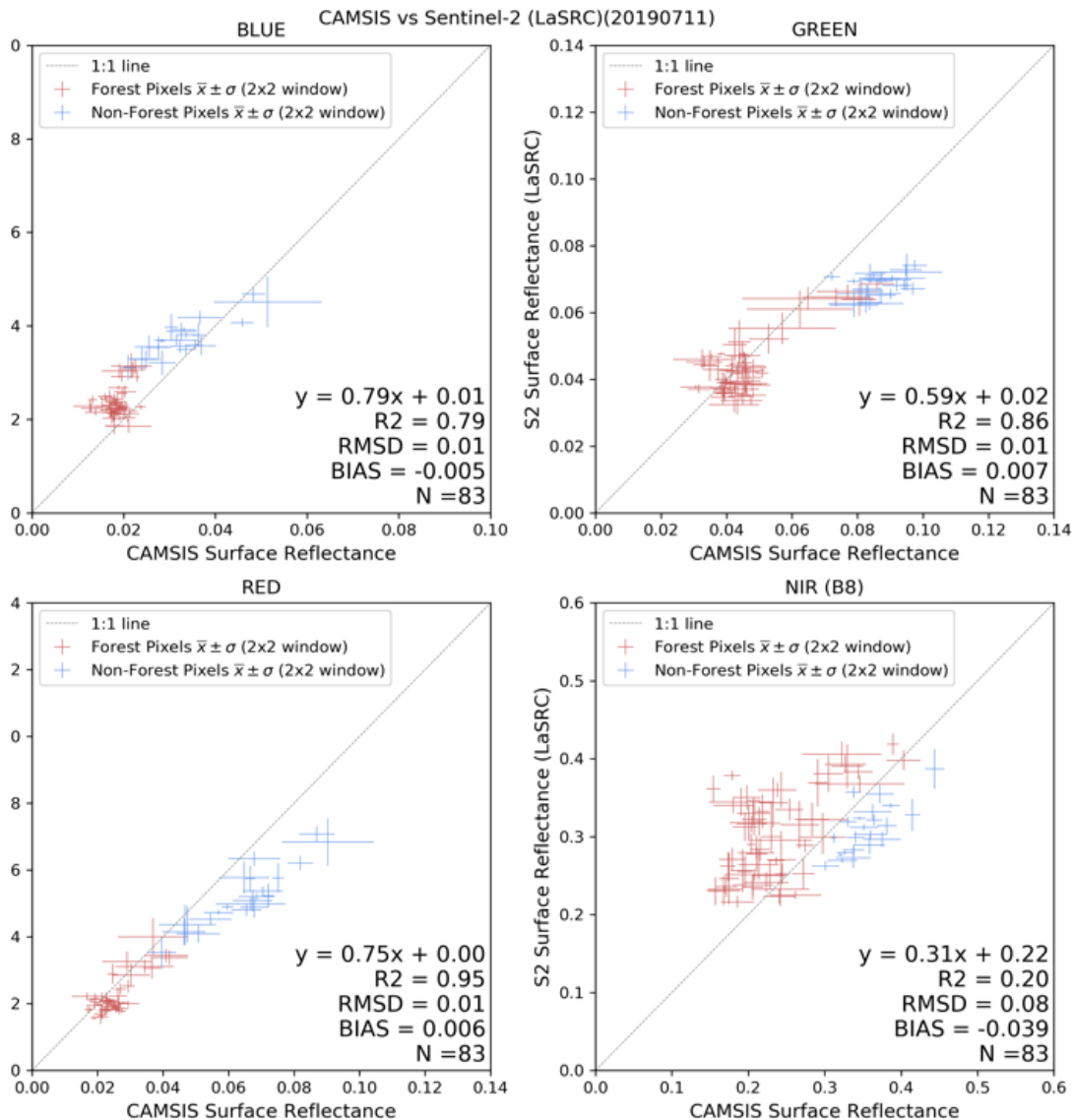
Calibrated and Merged

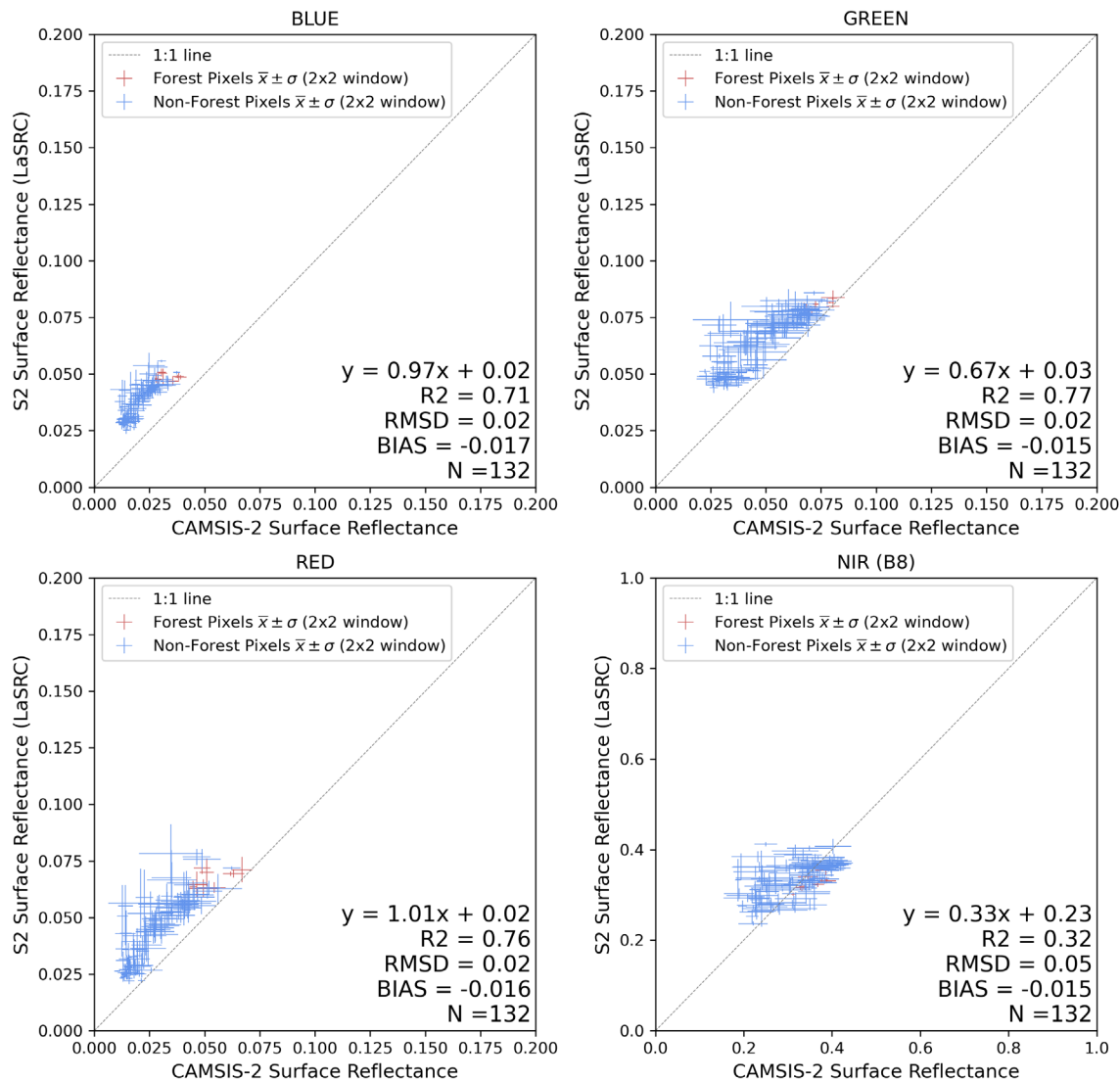


CAMSIS Data processing

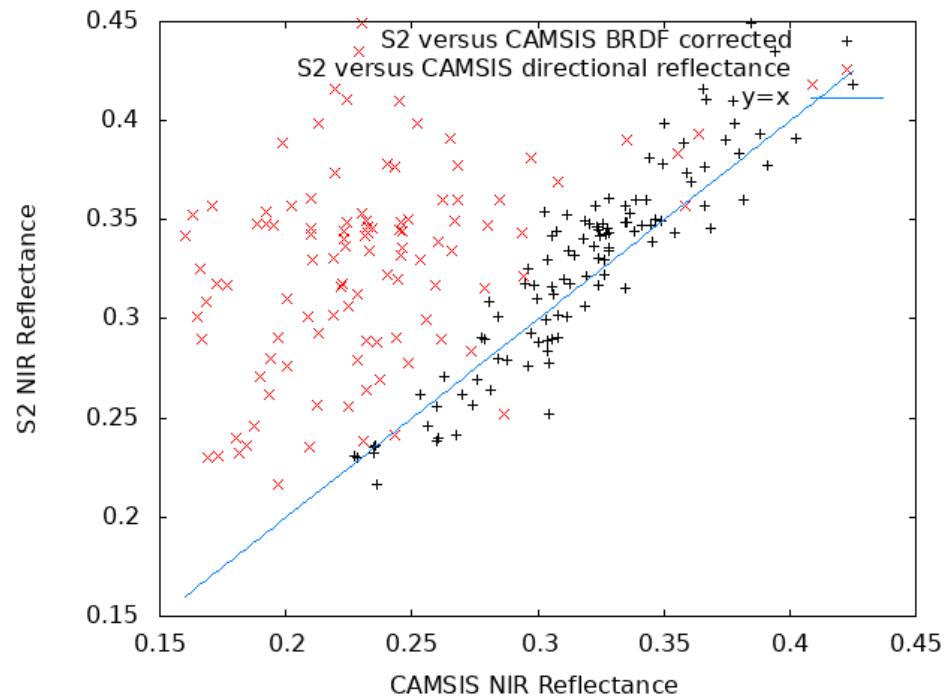


First results from CAMSIS on Sentinel 2

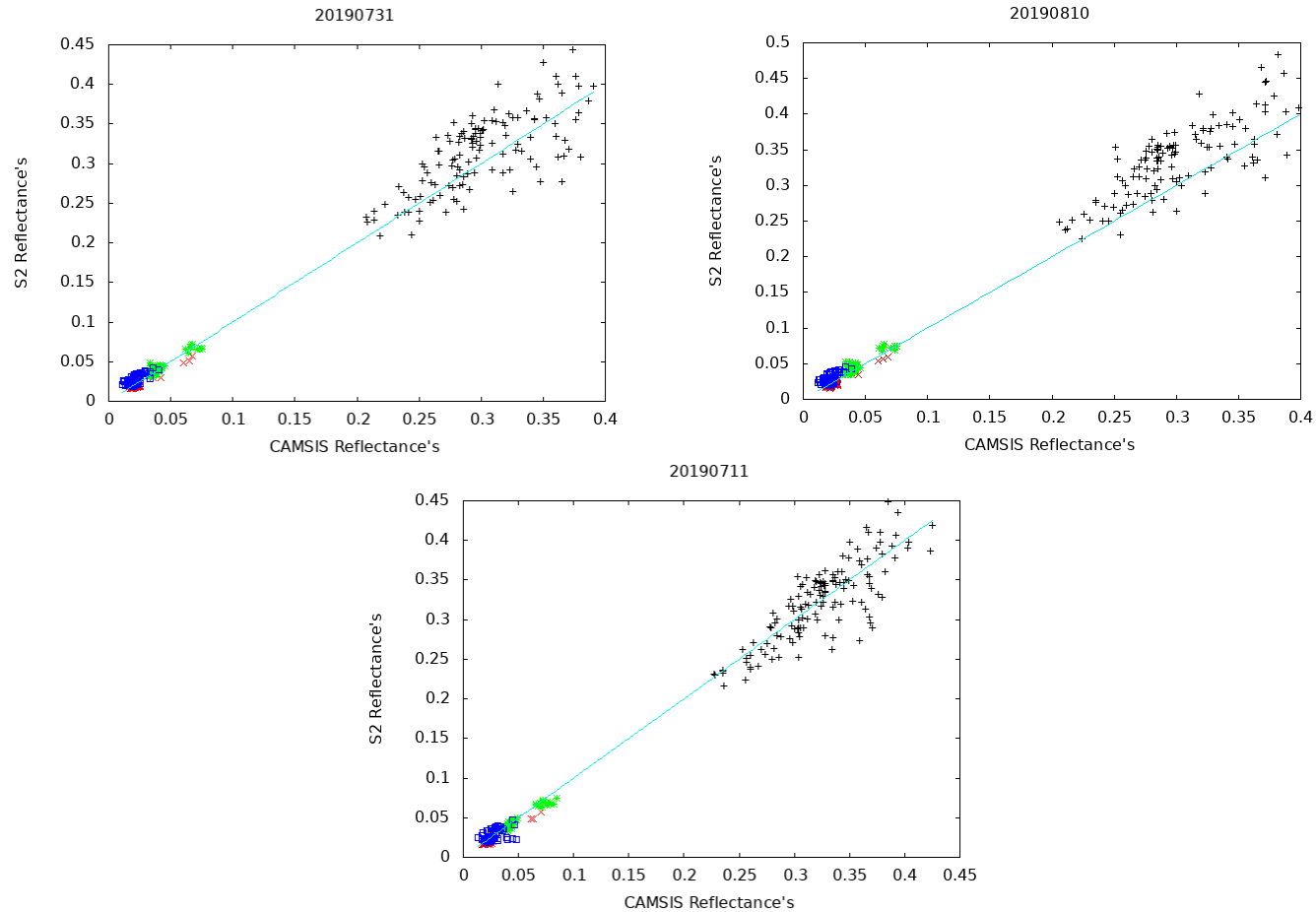




Applying BRDF correction to CAMSIS (NIR)



BRDF applied and starting quantitative comparison



El Palmar Super Site



SKYCAM 2



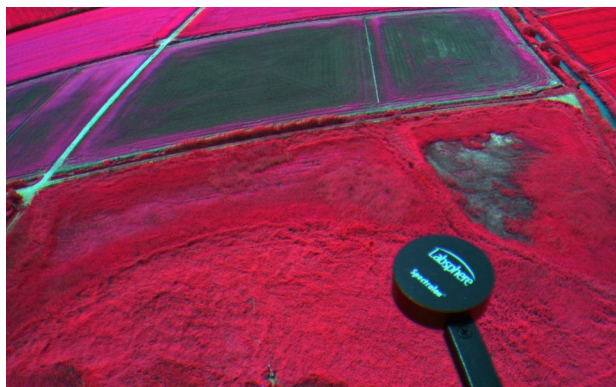
SKYCAM 1



AERONET



CAMSIS 1-2 "launch"



CAMSIS 2 NIR-RG



CAMSIS 1-2 installed

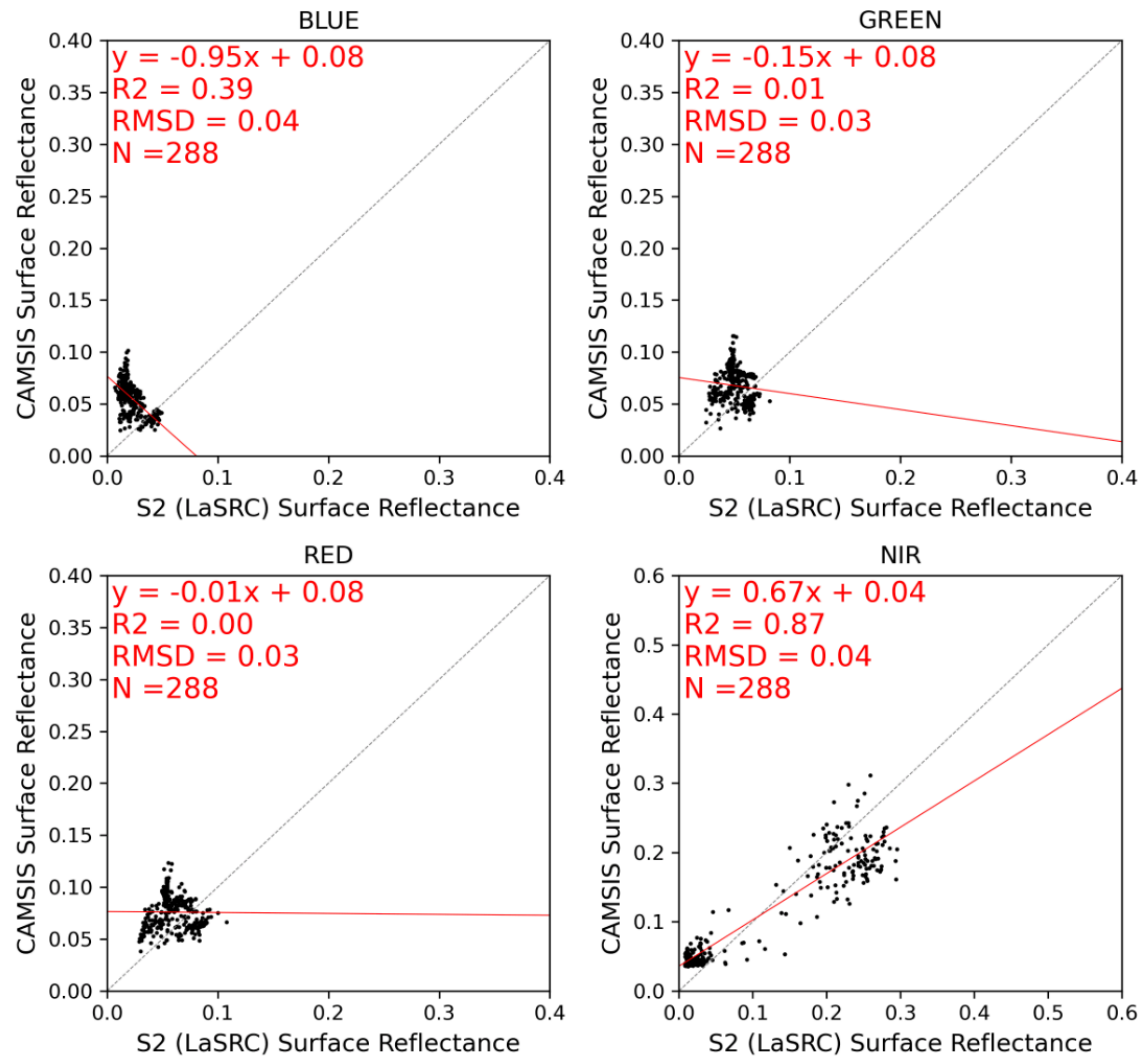


CAMSIS 2 RGB

El Palmar Super Site, First CAMSIS Results



CAMSIS Time: 20231106T104501



Conclusions

- Surface reflectance (SR) algorithm is mature and pathway toward validation and automated QA is clearly identified.
- Algorithm is generic and tied to documented validated radiative transfer code so the accuracy is traceable enabling error budget.
- The use of BRDF correction enables easy cross-comparison of different sensors (MODIS, VIIRS, AVHRR, Landsat, Sentinel 2, Sentinel 3...).
- We are proposing a complete package for Surface reflectance validation at high spatial resolution (Landsat, S2, AERONET, CAMSIS, SKYCAM).